UNIVERSITY OF CALIFORNIA
RIVERSIDE

Development and Application of a Reductive Titanium Dioxide Catalyst for Nitrate Removal

A Thesis submitted in partial satisfaction
of the requirements for the degree of

Master of Science

in

Environmental Toxicology

by

Matthew Lee Chen

December 2015

Thesis Committee:
Dr. Haizhou Liu, Chairperson
Dr. Sharon Walker
Dr. Jay Gan

The Thesis of Matthew Lee Chen is approved:

_____

_____

_____

Committee Chairperson

University of California, Riverside

Acknowledgements

There are many people helping me through the M.S study that I would like to thank. First of all is my advisor, Professor Haizhou Liu. During these two years, he has provided guidance and valuable advice toward by experiments and writings. I would also like to thank my dissertation committee for their valuable suggestions and comments to my work and writings: Professor Sharon Walker (Chemical and Environmental Engineering Department) and Professor Jay Gan (Environmental Science Department). I would also like to thank all the professors for the classes they taught.

I am also thankful to all the help and encouragements from collaborators, undergraduate student assistants, and other students in Dr. Liu's lab. Special thanks to several collaborators in the chemical sciences department: Dr. Yadong Yin and Dr. Wenshou Wang.

This thesis research was financially supported by the T32 research grant for environmental toxicology. Support was also provided through CEE startup fund and the UC Riverside center for catalysis.

ABSTRACT OF THE THESIS

Development and Application of a Reductive Titanium Dioxide Catalyst for Nitrate Removal

by

Matthew Lee Chen

Master of Science, Graduate Program in Environmental Toxicology
University of California, Riverside, December 2015
Dr. Haizhou Liu, Chairperson

A large population in the United States relies on groundwater as the drinking water source. One typical pollutant of groundwater is nitrate (NO_3^-). Individuals that have consumed water with high levels of nitrate are at the risk of methemoglobonemia. Due to the prevalence of nitrate contamination in groundwater, various methods have been developed to remove nitrate. These methods include ion exchange, reverse osmosis, and biological denitrification. Photocatalysts have been used for water treatment but are conventionally used for oxidative treatment of pollutants in water. Usage of TiO_2 for reductive treatment requires the addition of organic solvent for use as an external hole scavenger. Organic solvent addition to water makes the water undrinkable. The objective of this study was to develop a reductive TiO_2 photocatalyst and apply it to treat nitrate-contaminated groundwater. One type of synthesized TiO_2 was capped with diethylene glycol (DEG) solvent and also doped with barium (Ba). The second type of TiO_2 catalyst was also synthesized with a DEG cap but did not have barium doping.

Doping of barium to the catalyst when DEG was present did not lead to increased nitrate reduction. DEG provided sufficient electrons to block photo-generated holes.

There existed an optimum combination of precursor concentration and heating time during hydrolysis.

A catalyst dosage of 50 mg/L was determined to be the optimum dosage. Increasing the level of nitrate had a negative impact upon the performance of the catalyst as a result of increased hydroxyl radical generation and resulting consumption of photo-generated electrons. Other anions found in groundwater including sulfate, phosphate, carbonate, and chloride were shown to not produce a negative effect upon the performance of the catalyst.

Synthesized TiO_2 can also be applied to water sources that may be unsuitable for biological treatment due to the fragile nature of bacteria. The relatively little wasted generated from synthesized TiO_2 allows synthesized TiO_2 to be used for water sources in areas where there are limited options for wasted disposal.

Table of Contents

List of Figures

List of Equations

List of Tables

Chapter 1: Introduction

1.1 Nitrate Contamination in Groundwater

Groundwater is a vital water resource. Over 79.6 billion gallons of groundwater are used daily in the United States for drinking water supplies, irrigation, industry and other sectors.[1] Groundwater, however, is vulnerable to contamination of chemicals released from the surface. Nitrate is one of the most ubiquitous contaminants in groundwater.[2] Excessive levels of nitrogen compounds are introduced to soil through the agricultural, industrial and municipal sectors.[3] Many septic tank owners improperly dispose of nitrates, solvents and detergents into their septic tank systems.[3] The liquid effluent flows into a leaching or absorbing field to seep slowly and degrade naturally. Improper maintenance or construction of septic tanks can lead to leaching of these contaminants into groundwater.[4] Leachate high in nitrate concentration can seep from landfills into groundwater greatly increasing nitrate concentration levels.[4]

The state of California, for example, contains multiple areas in which nitrate concentrations are in excess of 45 mg/L as nitrate, the state-level MCL.[5] Areas with the highest levels of nitrate can reach upwards of 90 mg/L as nitrate.[5] The MCL of a chemical is the legally enforceable drinking water standard set by the US EPA on the basis of Safe Drinking Water Act .[6] The federal MCL for nitrate is 10 mg-N/L.[5]

The use of nitrogen-based fertilizers contributes significantly to the elevated levels of nitrate in groundwater.[7] Nitrogen fertilizer sales have increased by 300% in California over the last half a century with annual sales in excess of 0.6 million tons of

nitrogen in certain years.[7] It can be seen from Figure 1 that the amount of nitrogen based fertilizer used by the United States has increased steadily over the last 50 years.[8] Figure 1 also shows that nitrogen based fertilizers comprise the largest percentage of total fertilizers. The increasing use of nitrogen fertilizers can lead to increased levels of nitrogen compounds in the soil.[8]

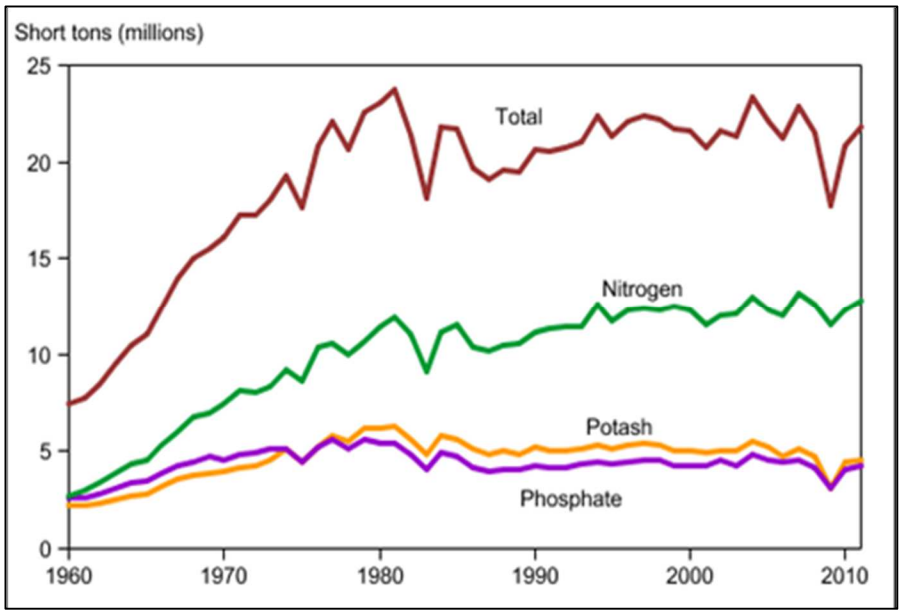

Figure 1. Fertilizer Use in the United States 1960-2010.[8] Nitrogen fertilizers have seen the greatest increase in usage from 1960-2010. As of 2010, the total amount of nitrogen fertilizers used is greater than the sum of potash and phosphate fertilizer used.

1.2 Health Effects and Toxicity of Nitrate

Human health effects due to consumption of nitrate-contaminated water have been linked with the symptom of methemoglobinemia,[9] which is associated with bluish skin along with lethargy and drowsiness.[10] The symptoms are a result of decreased delivery of oxygen resulting from increased levels of methemoglobin in the blood.

Methemoglobin is formed when the ferrous iron of hemoglobin is oxidized to ferric iron by digested nitrate.[11] Methemoglobin resulting from nitrate consumption is due to the accumulation of nitrite (NO_2^-) reduction by ferric iron of hemoglobin.[12] Infants and young children are more vulnerable to nitrate poisoning due to the more alkaline conditions in infant stomachs that promote growth of nitrate reducing bacteria.[10]

1.3 Existing Nitrate Removal Technologies

The removal of nitrate has become increasingly important because of the ubiquitous presence of nitrate in groundwater and the greater vulnerability of certain portions of the population. The high solubility and stability of nitrate makes it difficult to remove by several conventional water treatment systems including coagulation, lime softening and filtration.[13] More specialized treatment processes need to be employed for nitrate removal from drinking water. These processes include ion exchange, reverse osmosis and biological treatment. Each of these methods differs in terms of effectiveness, cost and simplicity of operation.

Ion exchange has been widely used for nitrate removal for drinking water treatment. This process applies anion exchange resins in a flow-through column where nitrate and other anions are adsorbed and exchanged for chloride or bicarbonate ions.[14] The operation of ion exchange treatment results in the depletion of resin exchange capacity. Consequently, the spent resin needs to be regenerated. A solution of highly concentrated sodium chloride must be passed over the resin to regenerate the exchange capacity.[15] The regeneration process generates a concentrated waste (*i.e.*, ion exchange brine) with extremely high levels of nitrate and other anions, resulting in the production

of a secondary waste. Disposal of the brine waste results in a large additional cost and limits the application of ion exchange in large scales.[16] The increased chloride concentration of the water after undergoing ion exchange also increases the corrosiveness of water and the risks of metal leaching into the distribution system.[17]

Furthermore, the efficiency of nitrate removal by the ion exchange is affected by other anionic constituents in the water.[18] High concentrations of sulfate can decrease the treatment efficiency due to the competitive adsorption between sulfate and nitrate. Standard ion exchange resins have a higher affinity for sulfate than nitrate, although it can be partially overcome by the use of a nitrate-selective resin.[19] Nitrate selective resins, however, are more costly.[19] Treatment of water with high organic content can also lead to fouling of the ion exchange resin, which reduces the efficiency of the process.[20]

Reverse osmosis is another process by which nitrate is removed from water. During reverse osmosis (RO) water is forced to cross a semi permeable membrane that filters out nitrate and other ions.[21] The RO process produces a permeate and a concentrate stream that contains high concentrations of chloride, sulfate, nitrate and bicarbonate. Chloride, nitrate and sulfate can increase to 7-8 times the concentration in the RO feed.[22] Disposal and management of RO concentrate is especially challenging for inland areas.[22]

Biological denitrification has also been widely applied for nitrate removal, especially for municipal wastewater.[23] Biological denitrification uses selective bacteria in anoxic conditions to utilize nitrate as the electron acceptor for microbial metabolism. The overall process reduces nitrate to nitrogen gas (N_2), as shown in Reaction 3:[24]

$$NO_3^- \rightarrow NO_2^- \rightarrow NO \rightarrow 0.5N_2O \rightarrow 0.5N_2 \qquad (1)$$

Both heterotrophic and autotrophic denitrifying bacteria can be involved in denitrification. Heterotrophic bacteria require organic substrates such as methanol, ethanol, and acetic acid as the electron donor.[24] Autotrophic bacteria require hydrogen or reduced sulfur (*i.e.,* thiosulfate) as the electron donor.[23] Biological denitrification is less sensitive to the presence of sulfate and organic matter compared to the ion exchange process. Albeit for the advantages, biological denitrification has slow reaction kinetics.[25] The start-up period for biological denitrification ranges between 3 and 6 weeks. Adequate solid retention time (SRT) needs to be provided to promote growth of slower growing denitrifying bacteria.[25] Typical SRT values can range from 15 days to 30 days.[26]

1.4 Nanotechnology for Nitrate Removal

New advances in nanotechnology have developed new processes in nitrate removal. Nanoscale zero valent iron (nZVI) is a method that uses zero valent iron (Fe^0) to reduce nitrate as shown in Equations 2-4.[27] The cost of nZVI method is low in comparison to conventional treatment methods, and nZVI is commercially available and non-toxic.[28]

$$4Fe^0 + NO_3^- + 10H^+ \rightarrow 4Fe^{2+} + NH_4^+ + 3H_2O \quad (2)$$

$$5Fe^0 + 2NO_3^- + 12H^+ \rightarrow 5Fe^{2+} + N_2 + 6H_2O \quad (3)$$

$$Fe^0 + NO_3^- + 2H^+ \rightarrow Fe^{2+} + NO_2^- + H_2O \quad (4)$$

Iron in the process is oxidized from zero valent state to its ferrous iron form. This method was shown to be able to remove up to 80% of nitrate in a recirculated flow through reactor.[27] Longer reaction times, up to 4 hours, are required to reduce higher percentages of nitrate.[29] During the reaction, parts of nZVI are converted into ferric

hydroxide.[29] Ferric hydroxide decreases surface contact between nZVI and nitrogen delaying the reaction.[29] Agglomeration of nZVI due to its colloidal characteristics limits its applications.[30]

There are multiple advantages for using TiO_2 to remove nitrate compared to other conventional treatment methods. TiO_2 can be applied to a wider range of water matrices. Water lacking organic compounds are difficult to treat using bacteria since additional organic compounds as carbon sources are needed for the bacteria.[35] Water that contains high levels of dissolved solids, sulfate and hardness are difficult to treat using ion-exchange due to precipitation during regeneration.[36] TiO_2 is also less expensive compared to reverse osmosis and ion exchange due to lower operating and maintenance costs. The amount of waste generated from using TiO_2 is significantly less than that generated when using reverse osmosis and ion exchange.[36]

Photocatalysts such as titanium dioxide (TiO_2) have traditionally been used for oxidative water treatment. The process of photocatalysis can be defined as the production of a catalyst from absorption of light.[31] TiO_2 is a semiconductor, and the positioning of the valence band and conduction band of a semiconductor allow for absorption of light and photocatalysis.[32] P25 TiO_2 has been used for degradation of air and water pollutants for many years.[37] Its excellent photocatalytic activity has allowed it to be used as a photocatalyst for the oxidation of many organic and inorganic compounds.[37] P25 is synthesized using high temperature flame hydrolysis of $TiCl_4$ in the presence of oxygen and hydrogen.[37] P25 is a mixed phase of anatase and rutile TiO_2.

Commercial manufacturers will advertise the ratio of anatase:rutile as 80:20, although this ratio will vary with different batches of P25.[37]

1.5 Photocatalytically Reductive Nitrate Removal

Traditional TiO_2 is not used for reductive treatment processes of organic contaminants. Traditional TiO_2 is used for photocatalytic degradation of pollutants in solution through a series of hydroxylation reactions initiated by hydroxyl radicals.[32] Hydroxyl radicals (·OH) are produced when holes in the valence band contact and oxidize water. [32] Electrons can react with oxygen to form superoxide ions ($O_2^{\cdot -}$). Superoxide ions react with water to from peroxide radicals (·OOH) which can react with H^+ to form additional hydroxyl radicals.[32] Hydroxyl radicals then initiate a series of oxidations reactions that lead to photodegradation of pollutants.[32] A disadvantage of using commercially available TiO_2 is the requirement of the presence of an organic compound to fill valence band holes. Formic acid is currently one of the most efficient hole scavengers for use with TiO_2.[37] Residual formic acid, however, in water systems is undesirable as it can comprise drinking water quality.

The semi-conductor, TiO_2, has a valence band and conduction band separated by a specific quantity of energy known as the band gap. For TiO_2, the band gap is 3.2 eV.[33] When TiO_2 is illuminated with photons of energy greater than 3.2 eV, an electron is excited from the valence band of TiO_2 to the conduction band.[33] A separated electron-hole pair is made that can be used for oxidation and reduction reactions. A key issue of

highly efficient titanium dioxide photocatalysis is the prevention of hole-electron recombination.

Using TiO_2 for reductive treatment requires the addition of an external hole scavenger. Typical hole scavengers are organic compounds. EDTA, citric acid, salicylic acid, formic acid, acetic acid, ethanol and methanol have been used as external hole scavengers.[34] The purpose of the hole scavenger is to donate electrons to photo-generated holes. Typically the amount of external hole scavenger added is therefore in excess. The addition of these organic compounds in excess to drinking water renders the water unfit for drinking.

Currently synthesized TiO_2 does not possess a structural capacity for hole scavenging. Therefore an external sacrificial electron donor must be added to scavenge holes.[38] During the course of the reaction, the external hole scavenger is consumed and eventually becomes depleted.[39] The alternative method of TiO_2 in this study is synthesizing TiO_2 with an internal hole scavenging capacity. This method of synthesis of TiO_2 is novel and advantageous because it eliminates reliance on external sacrificial electron donors.[38] The cycling performance of the synthesized TiO_2 can now be extended to many more cycles.[38]

1.6 Research Objectives and Hypotheses

The objectives of this study were:

(1) Synthesize titanium dioxide that can reduce nitrate without addition of an external hole scavenger;

Hypothesis 1: Synthesis of titanium dioxide with an internal electron donor will allow titanium dioxide to reduce nitrate without the need for an external hole scavenger. The internal electron donor will scavenge photo-generated holes through donation of electrons.[31] Photogenerated holes are blocked so that electrons in the conduction band are available for reducing nitrate.

(2) Evaluate the effect of catalyst dosage, synthesis parameters, and experimental conditions on catalyst performance;

Hypothesis 2: Synthesis parameters can be altered such that optimum performance of TiO_2 can be achieved. . Different volumes of water will affect the anatase:rutile ratio of crystals of TiO_2. This will result in differing performances for different volumes of water added. Insufficient heating time will yield TiO_2 with decreased performance

(3) Evaluate the performance of the catalyst toward reducing other contaminants.

Hypothesis 3: Catalyst dosage will affect the amount of nitrate reduced along with productdistribution. It is thought that increasing the level of catalyst will increase the amount of electrons available for reduction of nitrate. More electrons will lead to nitrogen being reduced further

Chapter 2: Materials and Methods

2.1 Synthesis of TiO_2 Catalysts

2.1.1 Principles of DEG-capped TiO_2 Performance

Recombination of photogenerated electrons and holes of TiO_2 negatively affects the performance of the catalyst. Various methods have been attempted to overcome the recombination of holes and electrons. One successful method is the addition of a hole scavenger to the reaction system.[31] The hole scavenger during the photocatalytic reduction process donates electrons to photogenerated holes and is oxidized. Organic compounds such as methanol, ethanol, oxalic acid, acetic acid and formic acid have all been used as hole scavengers.[34] Hole scavengers that must be added separately are referred to as external sacrificial electron donors (SED).[38] More recently there has been work to create hole scavengers that can be incorporated as part of the catalyst, eliminating the need for separate addition. This study utilized solvent used during synthesis of TiO_2 as the organic hole scavenger. Diethylene glycol (DEG) was used as the solvent due to the high temperature required for synthesis of the nanoparticles. During the synthesis of TiO_2, the DEG solvent binds to the surface of the newly forming TiO_2 nanoparticles as shown in Figure 2. DEG becomes incorporated into the structure of the TiO_2 nanoparticles and is now the SED. This eliminates the need for addition of an external hole scavenger.

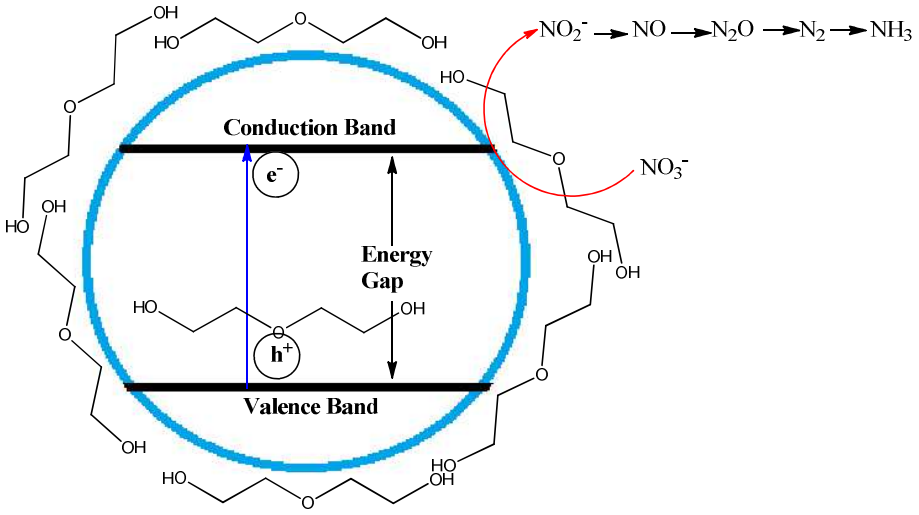

Figure 2. Depiction of DEG-capped catalyst. Diethylene glycol (DEG) donates electrons to the hole in the valence band, blocking recombination of the electron in the conduction band with the hole. The electron is free to reduce nitrate to nitrite and eventually to ammonia**.**

2.1.2. Principles of Ba-doped TiO_2 Performance

The purpose of synthesizing barium-doped titanium dioxide is the creation of a catalyst with an internal sacrificial electron donor. The internal sacrificial electron donor (SED) of the catalyst eliminates the need for addition of a separate external sacrificial electron donor such as formic acid or ethylene glycol. Barium ion has a valence of +2 while the titanium ion of TiO_2 has a valence of +4. When titanium dioxide is doped with barium, some of the titanium ions are replaced with barium ions in the crystal structure. Titanium being replaced with barium forms oxygen vacancies to maintain charge neutrality. For instance, if two titanium (+4) ions are exchanged for two barium (+2) ions, two oxygen vacancies are created.[40] Absent oxygen in the surface of TiO_2 results in

electrons localized in an oxygen vacancy state that can form a donor level in the electronic structure of TiO_2. The oxygen vacancies produced from barium doping can then scavenge the photogenerated holes from UV irradiation.[40] Figure 3 shows that DEG is also attached to the surface of barium doped TiO_2. DEG in Ba-doped TiO_2 also acts as a sacrificial electron donor (SED) along with the barium. Ba-doped TiO_2 possesses two different methods by which photogenerated holes can be blocked.

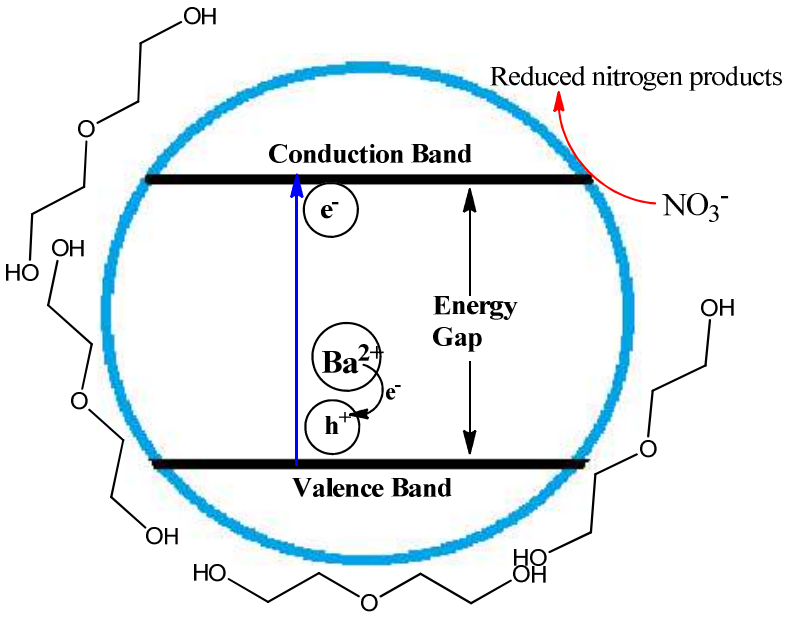

Figure 3. Depiction of barium-doped catalyst. Barium blocks the hole in the valence band and prevents recombination of the electron from the conduction band with the hole. Electrons in the conduction band reduce nitrate to nitrite and eventually to ammonia

2.1.3 Synthesis of TiO_2-Barium Doped

To synthesize Ba-doped TiO_2, 0.2 mL of titanium chloride ($TiCl_4$) in 20 mL of diethylene glycol solvent (DEG) was heated to 100 ^oC. Next, a 2-mM solution of barium chloride ($BaCl_2$) and H_2O (volume varied between 0.2 and 10 mL) were added to the solution and heated for two hours to a final temperature of 220^oC. These steps are illustrated in Figure 4. The concentration of $BaCl_2$ ranged from 66 mM to 98 mM dependent upon the volume of water added. The concentration of $TiCl_4$ ranged from 60 mM to 90 mM. The duration of the entire heating process was 2-6 hours. Not all Ba^{2+} can be doped in TiO_2. The molar ratio of Ti:Ba in the final product was 1: 0.012.

The solution after synthesis was first separated to two centrifuge tubes. Each tube contained about 10 ml solution to which 15 mL of 13.6 M acetone was added. The supernatant was removed after centrifugation at 5000 G for 10 minutes. This was followed by another addition of 25 ml of acetone into the tubes. The particles were sonicated to disperse. Then, the solutions in the two tubes were combined. After centrifugation and removal of the supernatant, another 25 ml acetone was added. After sonication, the solution was centrifuged at 11000 rpm for 5 minutes. The solution is centrifuged again at 9000 rpm for 5 minutes. Then, the supernatant was removed. Air was blown to dry the sample to a certain degree (not completely dry). Water was added to disperse the sample. Water was evaporated continuously in elevated temperature, from 120°C to 220°C.

2.1.4 Synthesis of TiO_2- DEG Capped

To synthesize DEG-capped TiO_2, 0.2 mL of titanium chloride ($TiCl_4$) in 20 mL of diethylene glycol solvent (DEG) was heated to 100 ^oC. Next 0.2-10 mL of water were added to the solution and heated to a final temperature of 220 ^oC. These steps can be seen in Figure 5. The concentration of $TiCl_4$ ranged from 60 mM to 90 mM depedent upon the volume of water added. The duration of the entire heating process was 2-6 hours.

The solution after synthesis was first separated to two centrifuge tubes. Each tube contained about 10 ml solution to which 15 mL of 13.6 M acetone was added. The supernatant was removed after centrifugation at 5000 G for 10 minutes. This was followed by another addition of 25 ml of acetone into the tubes. The particles were sonicated to disperse. Then, the solutions in the two tubes were combined. After centrifugation and removal of the supernatant, another 25 ml acetone was added. After sonication, the solution was centrifuged at 11000 rpm for 5 minutes. The solution is centrifuged again at 9000 rpm for 5 minutes. Then, the supernatant was removed. Air was blown to dry the sample to a certain degree (not completely dry). Water was added to disperse the sample. Water was evaporated continuously in elevated temperature, from 120°C to 220°C.

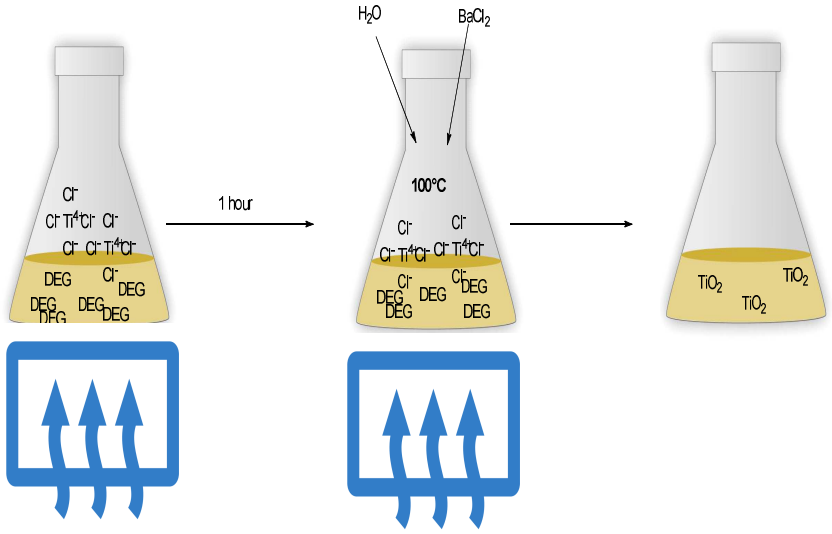

Figure 4. Synthesis of barium doped catalyst. To a reaction mixture flask, 0.2 mL of titanium chloride ($TiCl_4$) was added to 20 mL of diethylene glycol (DEG). This mixture was heated for one hour to 100°C. Next, 2 mmol of barium chloride ($BaCl_2$) was added along with 0.2-10 mL of water (H_2O). The resultant mixture was heated to temperature 220°C.

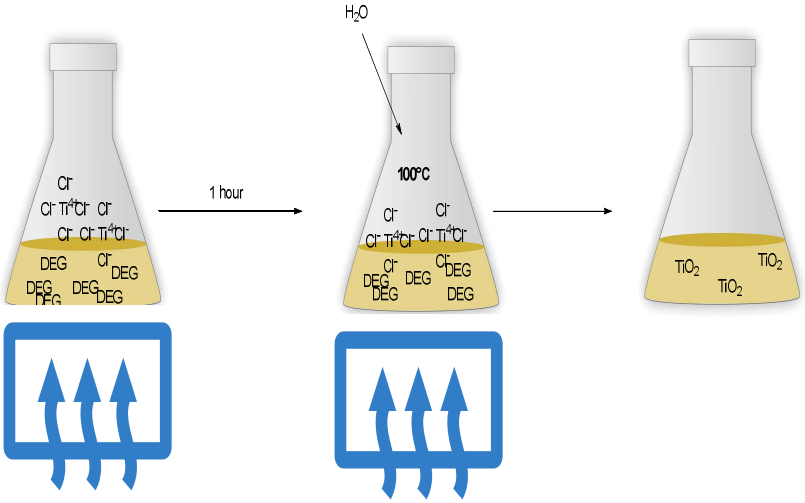

Figure 5. Synthesis of DEG-capped catalyst with no barium doping. To a reaction mixture flask, 0.2 mL of titanium chloride ($TiCl_4$) was added to 20 mL of diethylene glycol (DEG). This mixture was heated for one hour to 100°C. Next, 0.2-10 mL of water (H_2O) were added. The resultant mixture was heated to temperature 220°C

2.2 Set-up of photochemical experiments with synthesized TiO_2

2.2.1 Photochemical reactor Preparation

A 7836 Photochemical Safety Reaction Cabinet (ACE Glass Inc., Vineland, NJ) was used to host the quartz reactors and UV lamp while the experiment was running. Prior to the experiment, a 60 CFM exhaust fan was turned on and allowed to run for 30 minutes to allow the lamp to warm up to its full power before the experiment begins. This ensures that the lamp will be at a constant irradiance power for the duration of the experiment. The 60 CFM fan was also kept on for the entirety of the experiment to prevent overheating. The temperature of the experiments was maintained at 30° C.

2.2.2 Phosphate Buffer Preparation

To create a 500 mL 600 mM phosphate buffer stock solution, a mixture of 250 mL of 860 mM sodium phosphate dibasic anhydrate (Na_2HPO_4) and 250 mL of 340 mM sodium phosphate monobasic monohydrate ($NaH_2PO_4 \cdot H_2O$) was prepared, to give a final pH of 7.2. The mixture was sonicated for 20 minutes. To create a 500 mL of 300 mM phosphate buffer stock solution, a mixture of 250 mL of 420 mM sodium phosphate dibasic anhydrate (Na_2HPO_4) and 250 mL of 180 mM sodium phosphate monobasic monohydrate ($NaH_2PO_4 \cdot H_2O$) was prepared, to give a final pH of 7.2. To create a 500 mL 900 mM phosphate buffer stock solution, a mixture of 250 mL of 1280 mM sodium phosphate dibasic anhydrate (Na_2HPO_4) and 250 mL of 520 mM sodium phosphate monobasic monohydrate ($NaH_2PO_4 \cdot H_2O$) was prepared, to give a final pH of 7.2.

Figure 6 shows the reduction of nitrate with phosphate buffer present and phosphate buffer absent. The results show that the catalyst performs as well as when phosphate buffer is present as when phosphate is not present. The presence of phosphate does not interfere with the catalyst in reducing nitrate.

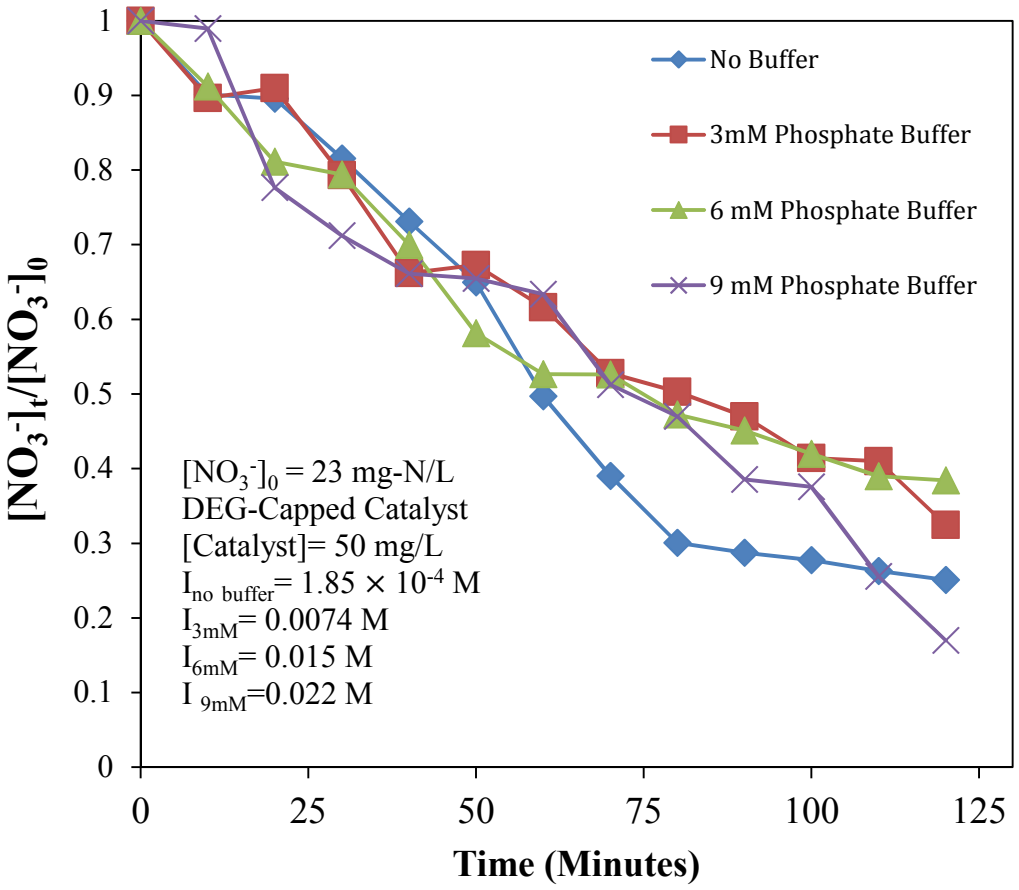

Figure 6. Photocatalytic reduction of nitrate using TiO_2 with and without phosphate buffer**.** Initial NO_3^- concentration was 23 mg-N/L. DEG-capped TiO_2 concentration was 50 mg/L.

2.2.3 Sample Preparation

A 10x dilution of the stock solution was performed. Two 5 mL samples from the 1000 mg/L NO_3^- stock solution were transferred to two 50 mL centrifuge tubes. Two 0.5 mL samples from the 600 mM phosphate buffer stock solution were added to the 50 mL centrifuge tubes. For 50 ppm catalyst concentration, 0.17 mL of 15,000 ppm catalyst stock solution was added to each of the centrifuge tubes. Millipore water was used to fill each centrifuge tube to the 50 mL mark. The centrifuge tubes and contents were centrifuged at 5000 rpm for 15 minutes. The contents of the centrifuge tubes were then transferred to 10 8 mL quartz tubes.

2.2.4 UV Experiments

Quartz tubes with samples were placed in a 7891 turntable UV reactor that rotated throughout the experiment duration**.** An ACE-Hanovia medium pressure quartz mercury arc lamp (ACE Glass Inc., Vineland, NJ**)** was used for the studies. Figure 7 shows that there are peaks in the photons/sec measurement for the medium pressure lamp below 380 nm. The band gap of anatase phase TiO_2 is 3.2 eV, which corresponds to 388 nm.[33] The medium press lamp was able to provide light of sufficient energy to promote electrons from the valence band of TiO_2 to the conduction band. The medium pressure mercury lamp operated at 135 volts and 3.8 amps and had an electrical power rating of 450 watts. The arc length of the lamp was 4.5 inches. The Hg Lamp was placed in an immersion well during the experiment and also during non-use.

A 1 g/L nitrate stock solution was prepared using the salt sodium nitrate ($NaNO_3$). A quantity of 0.34 g of $NaNO_3$ was measured and added to a 250 mL glass bottle. A 250

mL volumetric flask was used to measure out 250 mL of Millipore water and transfer to the 250 mL glass bottle. The solution was sonicated for 15 minutes.

Samples were taken every 30 minutes using a sacrificial sampling technique where one quartz tube was removed and its contents filtered into a 15 mL centrifuge tube for storage. The filter used was a Hydrophilic PVDV 0.22 um pore size filter (Bonna-Agela Technologies Inc, Wilmington, DE). After filtering the sample was stored in the 15 mL centrifuge tube for use in the IC after the experiment was completed. If the samples were to be stored overnight, they were transferred to the refrigerator.

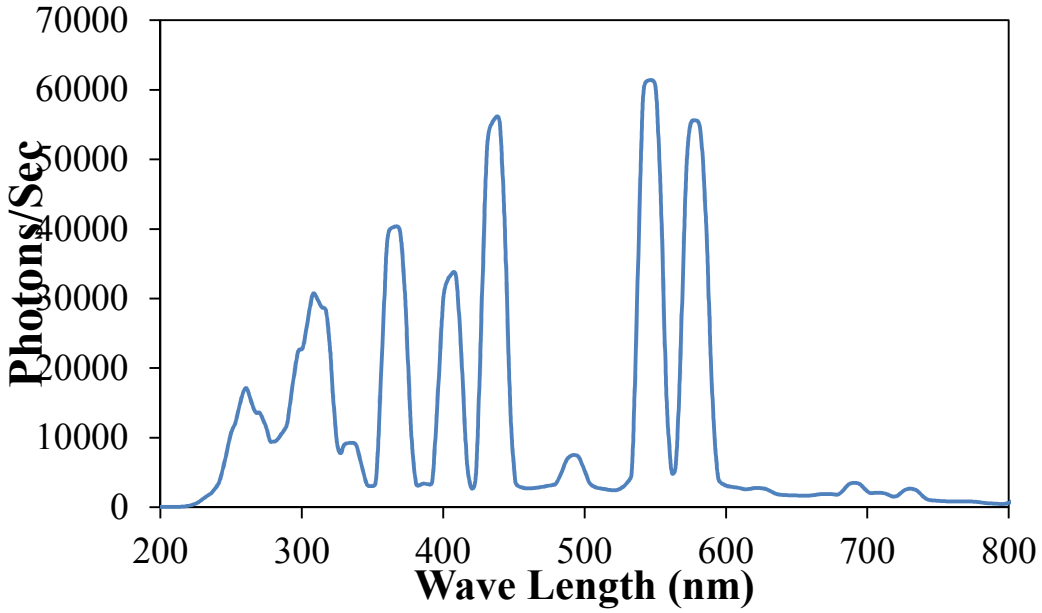

Figure 7. Photons/sec for Hg Lamp vs. Wavelength (nm). The photons/sec are shown as a function of wavelength (nm).

2.3 Analytical Methods

Concentrations of nitrate and nitrite were analyzed using ion chromatography (IC) by a Thermo Scientific DX-120 Ion Chromatograph DS4-1 (Thermo Fisher Scientific, Sunnyvale, CA 94086). The eluent used for IC measurements was 4.5 mM Na_2CO_3 and 1.4 mM $NaHCO_3$. The flow rate was set at 0.86 mL/min. The column used was an anion column Dionex Ion Pac^{TM} AS22 RFIC (Thermo Fisher Scientific, Sunnyvale, CA 94086). The dimensions of the column were 4x250 mm. The diameter of the beads were 6 um. The supermacro resin had a diameter of 11 um with a cross-linking value of 55%. 0.5 mL samples of filtered samples was pipetted into 0.5 mL AS-40 vials with CAP. Samples were loaded into treys of 8 using an autoloader.

IC chromatograms displayed three peaks corresponding to nitrate, nitrite, and phosphate. Nitrate displayed a peak at 8.4 minutes. Nitrite displayed a peak at 6.2 minutes. Phosphate buffer displayed a peak at 10.2 minutes.

2.3.1 Ammonia UV-VIS Measurement

A Horiba Aqualog (JOBIN YVON, New Jersey, NJ) UV-C with software version3.6 was used to measure ammonia concentration using the phenate method.[41]

2.3.2 Phenate Method for Determination of Ammonia[41]

The amount of ammonia was determined by using the Phenate Method. Five different reagents were created: A- Phenol Solution, B- sodium nitroprusside solution, C- alkaline citrate solution, D- sodium hypochlorite solution, and E- oxidizing solution. Reagent A was created using 9 mL of $\geq$ 89% liquefied phenol and 1 mL of ethanol. 0.1 g of sodium nitroprusside was dissolved in 20 mL of water to create reagent B. 200g of

sodium citrate with 10 g of sodium hydroxide were dissolved in 1000 mL of water to make reagent C. Reagent E was created by mixing 5 mL of reagent D with 20 mL of reagent C daily. Ammonium standards were created using ammonium chloride salt.

To measure ammonia, 5 mL of sample was mixed with 0.2 mL of Phenol Solution, 0.2 mL of sodium nitroprusside solution, and 0.5 mL of oxidizing solution. The sample was then covered with parafilm and removed from light for one hour to allow for color development. After one hour, absorbance is measured by UV spectrophotometer at the wavelength of 640 nm.

2.3.3 Measurement of Steady-State ·OH Concentration

Steady-state concentrations of hydroxyl radical ($[\cdot OH]_{ss}$) were calculated using phenol as a probe.[42] Quartz tubes with varying concentrations of nitrate (11-68 mg-N/L as Nitrate) and an initial concentration of phenol (100 uM) were exposed to light over 30 minutes in an ACE photochemistry cabinet (ACE Glass Incorporated, Vineland, NJ). A control experiment for direct photolysis of phenol was performed using an initial concentration of 100 uM with 0 ppm nitrate. Samples were taken every 3 minutes and transferred to a 15 mL centrifuge tube. A 2 mL sample from each centrifuge tube was taken and transferred to a clear autosampler HPLC vial for HPLC analysis. Samples were analyzed using an Agilent 1200 series HPLC (Agilent Technologies, Palo Alto, CA) equipped with a diode array detector. An Eclipse Zorbax XDB-C18 column (Agilent Technologies, Palo Alto, CA) was used with a mobile phase of 30% 10 mM formic acid

with 70% 19M acetonitrile at a flow rate of 1 mL/min and a detection wavelength of 254 nm.

Phenol decay was modeled as a pseudo first order reaction with respect to phenol. A graph of ln [pheno] *vs.* time with no nitrate present is plotted. A linear regression is performed through the data points as shown in Equation 5. The rate constant k_{direct} in Equation 6 is calculated by multiplying the slope of the line of best fit from Equation 5 by -1. A graph of ln [phenol] *vs.* time with nitrate present is plotted. A linear regression is performed through the data points as shown in Equation 7. The rate constant $k_{observed}$ in Equation 8 is calculated by multiplying the slope of the line of best fit from Equation 7 by -1. The rate constant $k_{observed}$ is defined in Equation 9 to be the sum of $k_{intrinsic}$ and $k_{direct.}$ Subtracting k_{direct} from $k_{observed}$ yields the rate constant $k_{intrinsic}$. Equation 10 defines the rate constant k_{phenol} to be equal to the product of $k_{intrinsic}$ and [HO·] steady state radical concentration. The rate constant k_{phenol} has been calculated and defined in Equation 11. $[HO\cdot]_{ss}$ is calculated by dividing k_{phenol} by $k_{intrinsic}$ as shown in Equation 12.

$$ln\ [\text{phenol}]_t = slope \times t + ln[\ phenol]_0 \quad no\ nitrate\ present \quad (5)$$

$$-1\ \times slope_5 = k_{direct} \quad (6)$$

$$ln\ [phenol]_t = slope\ \times t + ln[\ phenol]_0 \quad (7)$$

$$-1\ \times\ slope_7 = k_{observed} \quad (8)$$

$$k_{intrinsic} + k_{direct} = k_{observed} \quad (9)$$

$$k_{intrinsic} \times [\cdot OH]_{ss} = k_{phenol} \quad (10)$$

$$k_{phenol} = 1.4 \times 10^{10}\ M^{-1}s^{-1} \quad (11)^{42}$$

$$[HO\cdot]_{ss} = k_{phenol}\ /k_{intrinsic} \quad (12)$$

Chapter 3: Results

3.1 Comparison of Synthesized Catalysts

The performances of the three catalysts (Ba-doped TiO_2, DEG-capped TiO_2 and P25 TiO_2) were compared by measuring the removal of nitrate during a photochemical treatment of duration 120 minutes.

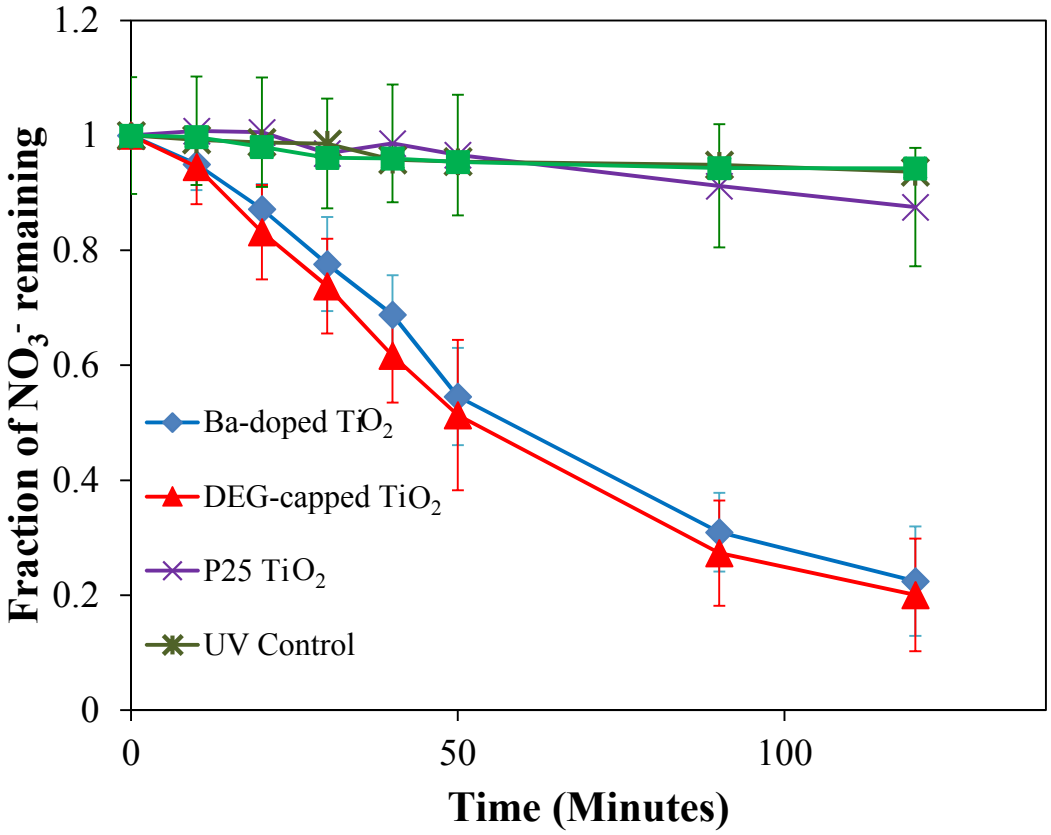

Figure 8. Impact of the catalyst type on NO_3^- reduction. The fraction of nitrate remaining is shown as a function of time for three catalysts: P25 TiO_2, DEG-Capped TiO_2, Ba-doped TiO_2. Initial NO_3^- concentration was 23 mg-N/L. Catalyst dosage was 50 mg/L. A medium pressure Hg-Lamp was used. The pH was maintained at 7.2 by 6 mM phosphate buffer. The ionic strength was 15 mM.

Commercially available P25-TiO_2 catalyst was used to represent TiO_2 designed for oxidative processes. The performance of P25 was compared to both diethylene glycol (DEG)- capped and barium-doped TiO_2 catalysts to determine the effects of custom synthesis upon the reductive power of TiO_2. A UV control and an adsorption control were also performed. Figure 8 shows nitrate levels did not decrease significantly in the UV Control. This indicates minimal nitrate reduction due to direct photolysis. Figure 8 also shows that nitrate levels did not decrease significantly in the Adsorption Control for the DEG-capped and Ba-doped catalyst showing that there was no significant adsorption of nitrate to either barium doped or DEG-capped catalyst. The amount of nitrate removed by both DEG-capped and barium doped catalyst was significantly higher when compared with P25-TiO_2 catalyst. Only 12.5% reduction of initial nitrate concentration was seen when P25-TiO_2 catalyst was used. The hole scavenger was observed to have a positive impact on the reductive properties of the TiO_2 catalyst. Ba-Doped TiO_2 and DEG-Capped TiO_2 produced similar levels of nitrate reduction. Usage of the Ba-doped TiO_2 led to 75% reduction of the initial nitrate concentration. Usage of the DEG-capped TiO_2 led to 79% reduction of the initial nitrate concentration.

A 2 sample t-test was performed using the data for barium-doped and DEG-capped TiO_2 to see if there was a difference in mean nitrate levels at each sampling point. The null hypothesis was that the mean nitrate level at each sampling point when Ba-doped TiO_2 was used was the same as the mean nitrate level at each sampling point when DEG-capped TiO_2 was used. The confidence limit was set at 95%. Each point was taken in triplicate corresponding to a degrees of freedom (DF) value of 2.

Table 1 T-statistics *vs.* time. A two-sample two-tailed t-test was performed at each sampling point to determine if the mean nitrate concentration values differed between the two catalysts.

Time (Minutes)	T-Statistic	Critical T value-Two Tail, 95% Confidence Limit
10	0.24	4.3
20	0.64	4.3
30	0.50	4.3
40	1.0	4.3
50	0.27	4.3
90	0.40	4.3
120	0.25	4.3

The two-tailed t-test was performed to compare the nitrate removal between DEG-capped TiO_2 and Ba-doped TiO_2. The critical value at a 95% confidence limit is 4.30. The values of the t-statistic are listed in table 1. At each time point, the absolute value of the t-statistic is less than the critical value of 4.30. Since the value of the t-statistic is less than the value of the critical value, the null hypothesis is not rejected at any time point. At all measured points, the mean value of nitrate concentration for Ba-doped TiO_2 does not differ significantly at the 95% confidence limit from the mean value of nitrate concentration for DEG-capped TiO_2.

The results of this experiment and the t-tests showed that the addition of barium as a doping agent did not lead to a significant increase in reduction of nitrate. Therefore, for further experiments, only the DEG-capped catalyst was utilized.

3.2 Impact of Synthesis Parameters

The synthesis of titanium dioxide (TiO_2) included titanium chloride ($TiCl_4$), water, and DEG. The concentration of $TiCl_4$ precursor was varied by altering the volume of water added during synthesis. The concentration of $TiCl_4$ ranged from 60 mM to 72 mM to 89 mM. The heating time during hydrolysis was also varied between two hours and six hours.

During the process of hydrolysis, water is used to break the bonds in the titanium chloride precursor. There was thought to be an optimum $TiCl_4$ concentration that would result in maximum performance of the catalyst. The predicted effect of excess water is shown in Figure 9A and 9B. Figure 9A shows the capping of TiO_2 by DEG molecules. DEG that is capped to the surface of TiO_2 can block photogenerated holes and maintain charge hole separation in the TiO_2. Figure 9B shows how excess water prevents DEG from forming a cap around TiO_2. DEG not bound to TiO_2 surface is unable to block photogenerated holes as well resulting in diminished charge-hole separation. This leads to diminished reductive ability of the catalyst.

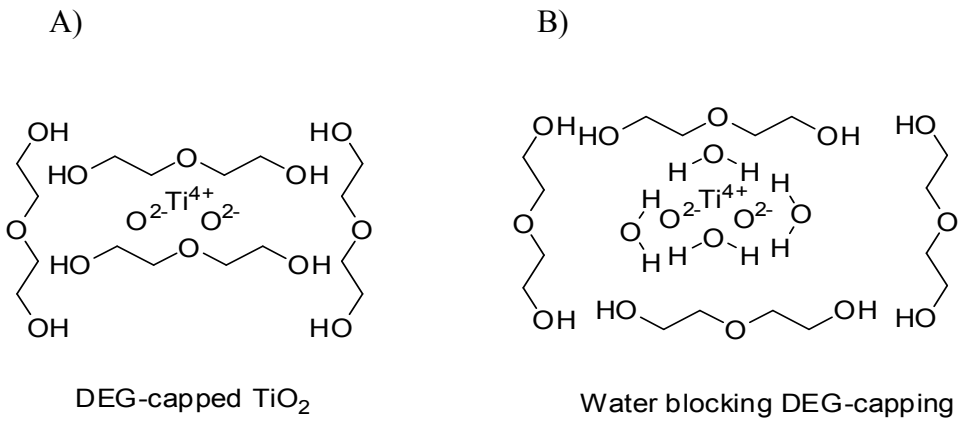

Figure 9. A) DEG is able to form a cap on TiO_2. B) Effect of excess water on DEG-capping of TiO_2. Excess water prevents diethylene glycol (DEG) from forming a cap around TiO_2.

The heating time during hydrolysis can affect the ratio of rutile to anatase phase in the TiO_2 crystals. The ratio of rutile to anatase increases as the heating time during hydrolysis increases.[43] This predicts that shorter heating times during hydrolysis will yield product with a higher percentage of rutile phase crystals.[43] Since rutile phase crystals have greater photoactivity compared to anatase phase crystals, increases in heating time past a certain time interval could have a negative effect on the performance of the catalyst.[43]

The natural log of nitrate concentration was plotted versus time in Figure 10. A linear regression was performed for each set of data in the different synthesis conditions. The value of $k_{apparent}$ for each of the catalysts synthesized was determined from the slope of the line of best fit. The resulting k values are listed in Table 1 from each set of synthesis conditions.

The optimum $TiCl_4$ concentration based on comparison of the first order rate constants was 89 mM. Decreasing $TiCl_4$ concentrations from this value resulted in lower

first order rate constants. The optimum heating time during hydrolysis based on first order constants was 3 hours. A 2 hour heating time during hydrolysis resulted in diminished nitrate reduction and lower first order rate constant. Increasing the heating time to 6 hours also resulted in diminished nitrate reduction and lower first order rate constant. The synthesis conditions chosen for subsequent experiments were 3 hour heating time during hydrolysis and 89 mM $TiCl_4$ concentration (condition #3 in Table 2).

Table 2 Pseudo first-order rate constant of different synthesis conditions. Concentration of DEG-capped catalyst was 50 mg/L. Initial NO_3^- concentration was 23 mg-N/L. A 6 mM phosphate buffer was used that maintained a pH 7.2. Ionic strength was 15 mM.

Condition	[$TiCl_4$] (mM)	Heating time during hydrolysis (hours)	k $\times 10^{-3}$ (s^{-1})
#1	60	6	0.7
#2	72	2	0.4
#3	89	3	2.0
#4	72	6	1.1

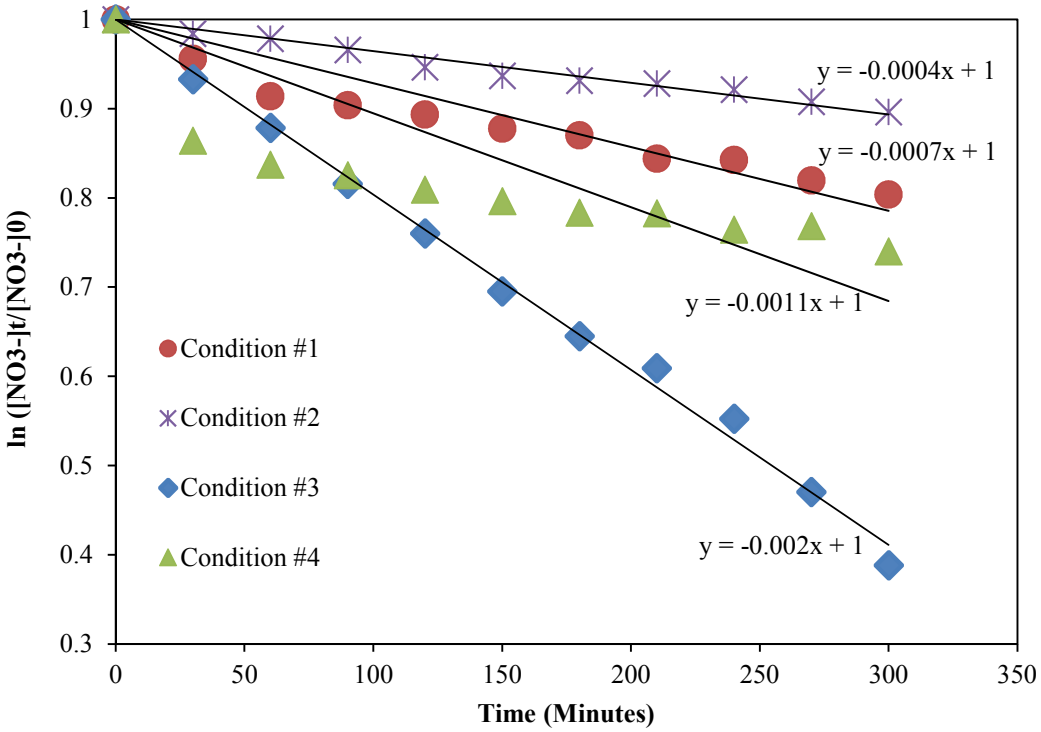

Figure 10. Impact of catalyst preparation on nitrate reduction rate constant. Initial NO_3^- concentration was 23 mg-N/L. A 6 mM phosphate buffer was used that maintained a pH 7.2. Ionic strength was 15 mM. DEG-capped catalyst concentration was 50 mg/L.

3.3 Impact of Catalyst Dosage

The reduction of contaminants with the catalyst was dependent upon the catalyst providing sufficient amount of electrons for reductive processes. The catalyst dosage was varied to determine the relationship between dosage value and performance of the catalyst. Three end-points were used to evaluate the catalyst performance: nitrate reduction, product distribution, and electron capacity. Figure 11 shows nitrate removal as a function of catalyst dosage.

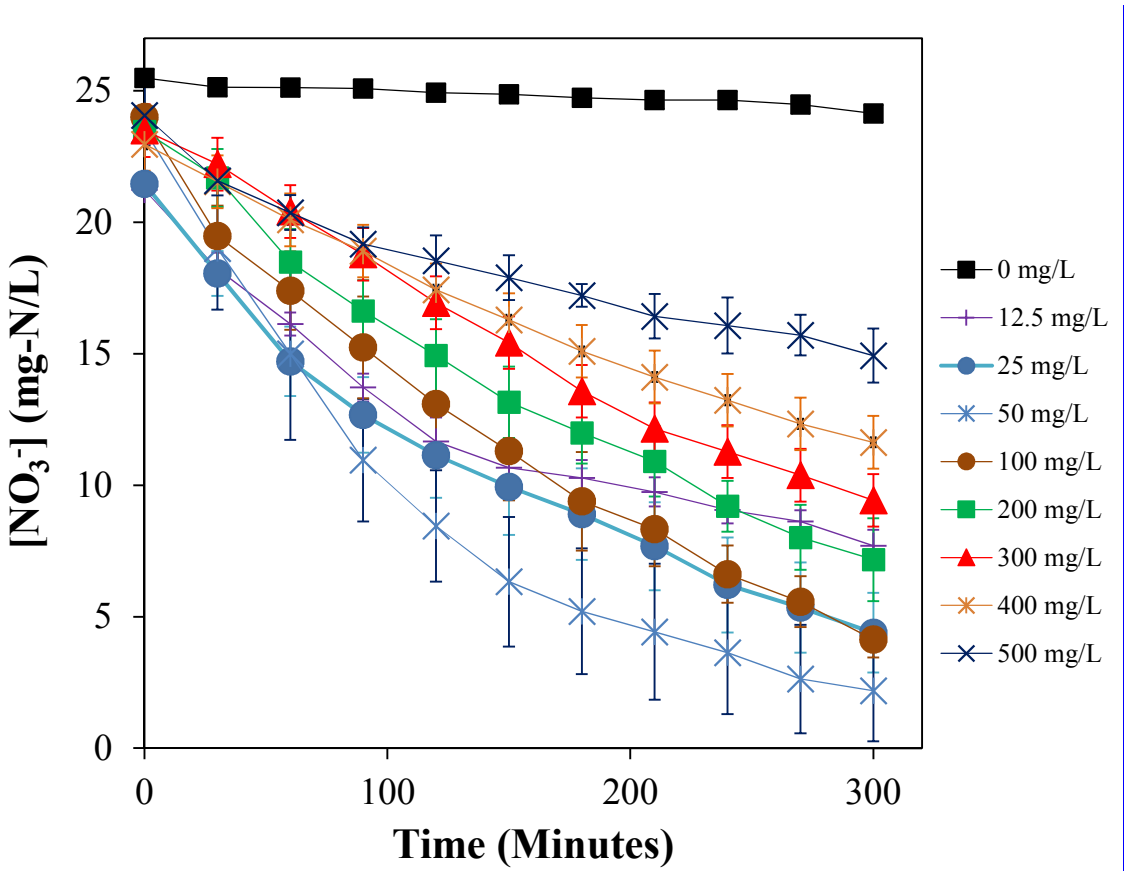

Figure 11. Impact of DEG-Capped -TiO_2 dosage on nitrate reduction. The amount of nitrate remaining is plotted as a function of time for catalyst dosages: 0, 25, 50, 100, 200, 300, 400, and 500 mg/L. Initial NO_3^- concentration was 23 mg-N/L. A 6 mM phosphate buffer was used that maintained a pH 7.2. Ionic strength was 15 mM. DEG-capped buffer of concentration 50 mg/L was used.

3.3.1 Impact of Catalyst Dosage on NO_3^- Reduction

Figure 11 shows that total nitrate removal was not directly proportional to dosage of catalyst. There seemed to be an optimal dosage at which nitrate removal was the greatest. Deviations from this optimum dosage resulted in decreasing nitrate removal. The optimum catalyst dosage with respect to nitrate reduction for this study was 50 mg/L. When a catalyst dosage of 50 mg/L was used, 90% of nitrate was removed in 300 minutes. When the dosage of catalyst was increased to 100, 200, 300, 400, and 500

mg/L, the percentage of nitrate removal decreased to 86%, 70%, 59%, 50%, and 38%, respectively. When the dosage of catalyst was deceased to 25 mg/L and 12.5 mg/L, the percentage of nitrate removal was decreased to 78% and 63%, respectively.

3.3.2 Impact of Catalyst Dosage on Product Distribution

Since nitrite is the compound responsible for the toxic effects seen from ingestion of nitrate, product selectivity and distribution needed to be evaluated. To evaluate product distribution nitrite and ammonia were directly measured. All measurements were taken in units of mg-N/L. Gaseous nitrogen species concentration (likely N_2) was calculated based on the following equation:

$$[Gaseous\ Nitrogen] = ([NO_3^-]_0 - [NO_3^-]_t) - [NO_2^-]_t - [NH_4^+]_t \quad (13)$$

$$[NO_3^-]_t = nitrate\ concentration\ at\ time\ t \quad (14)$$

$$[NO_2^-]_t = nitrite\ concentration\ at\ time\ t \quad (15)$$

$$[NH_4^+]_t = ammonia\ concentration\ at\ time\ t \quad (16)$$

$$[NO_3^-]_0 = initial\ nitrate\ concentration \quad (17)$$

The distributions of nitrate reduction products were plotted versus time for each catalyst dosage in Figures 12A and 12B. Figure 12A shows the product distribution for catalyst dosages of 12.5, 25, 50, and 100 mg/L. Figure 12B shows the product distribution for catalyst dosages of 200, 300, 400, and 500 mg/L.

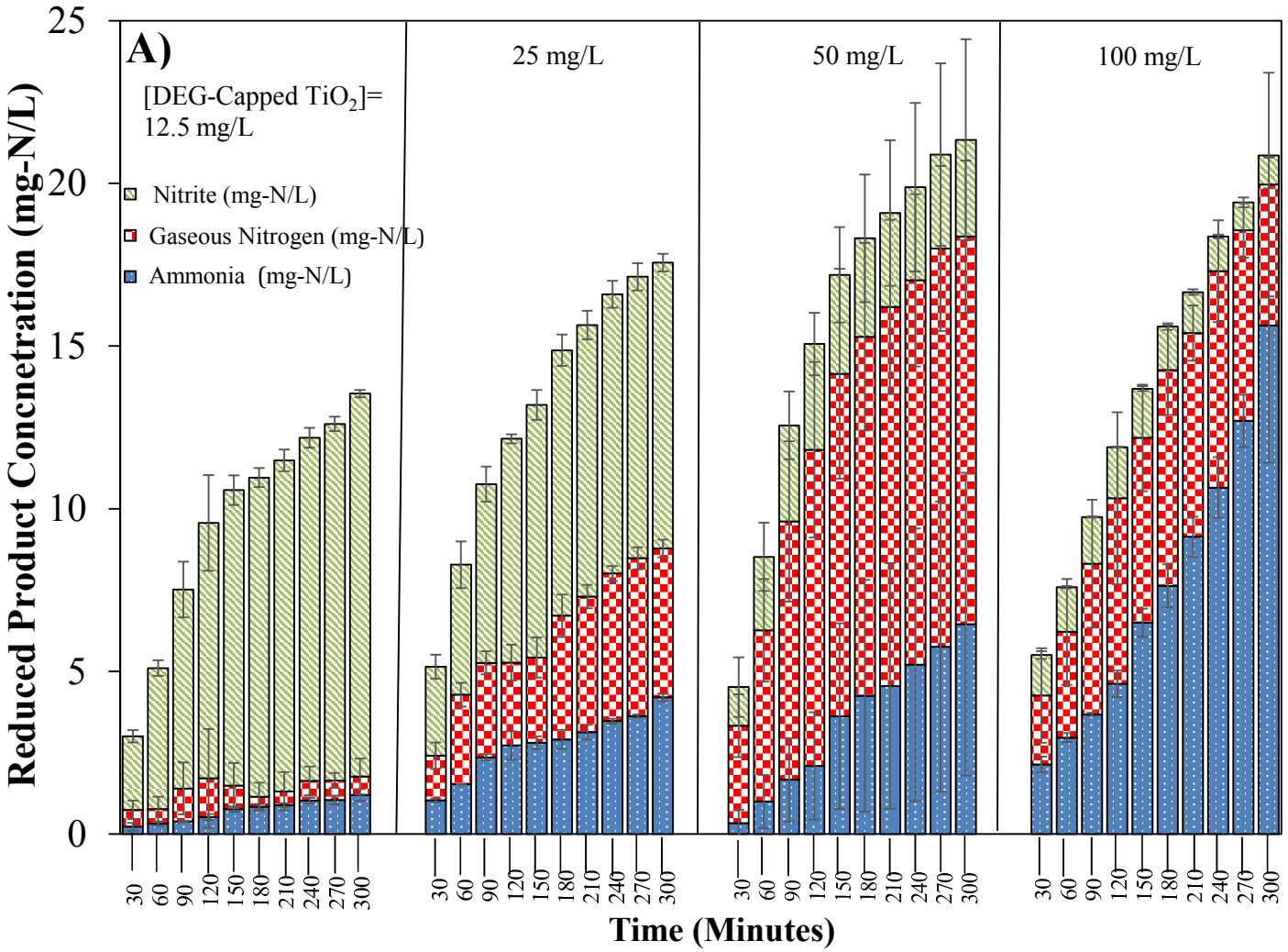
A)
[DEG-Capped TiO2]= 12.5 mg/L
Nitrite (mg-N/L)
Gaseous Nitrogen (mg-N/L)
Ammonia (mg-N/L)
25 mg/L
50 mg/L
100 mg/L
Reduced Product Concnetration (mg-N/L)
0
5
10
15
20
25
30
60
90
120
150
180
210
240
270
300
Time (Minutes)

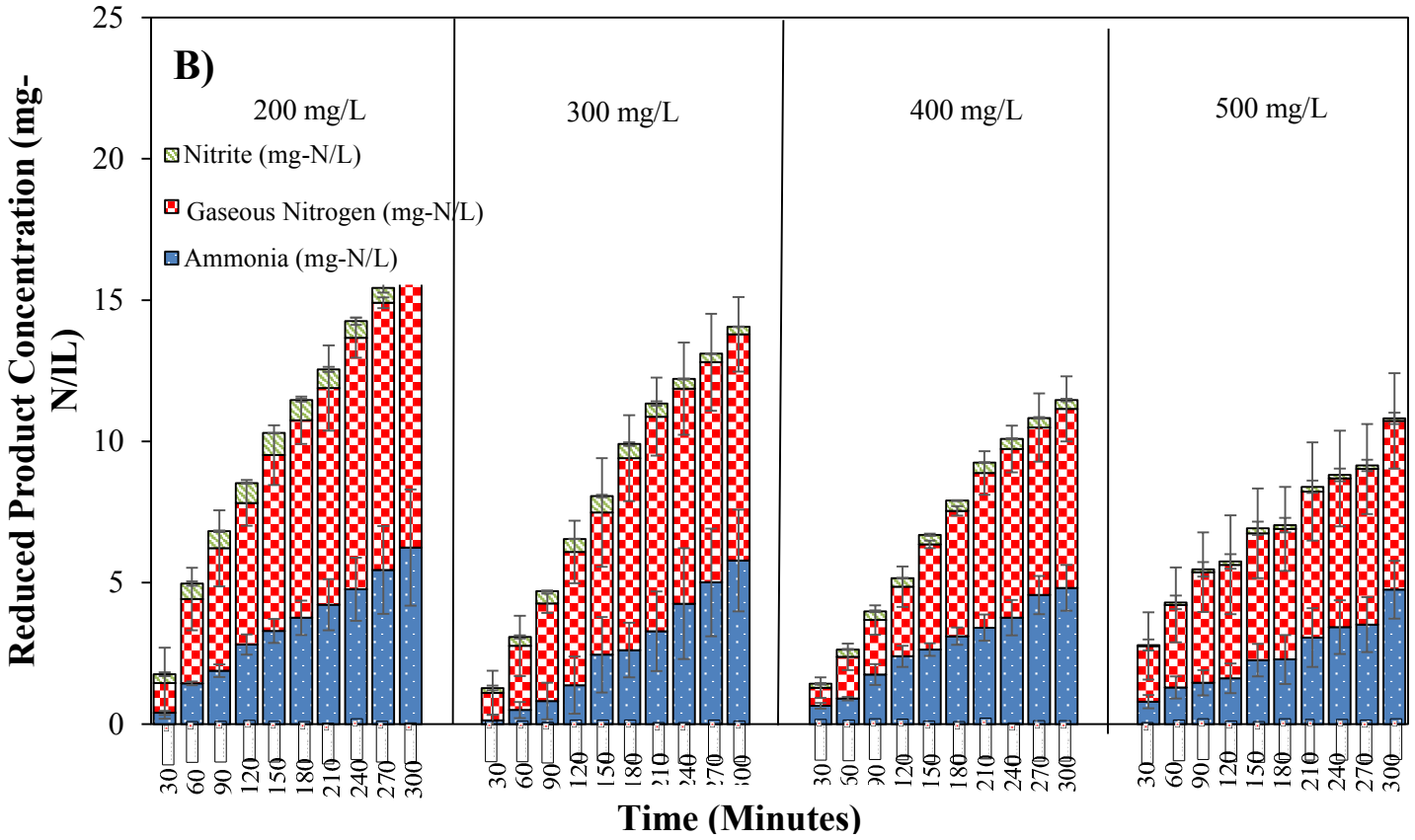

Figure 12. A) Impact of catalyst dosage (12.5-100 mg/L) on product distribution. B) Impact of catalyst dosage (200-500 mg/L) on product distribution. Blue bars represent ammonia formation. Red bars represent nitrogen gas formation. Green bars represent nitrite formation. 6 mM phosphate buffer used at pH 7.2 and ionic strength 15 mM. Initial nitrate concentration was 23 mg-N/L.

The sum of the checkerboard, dotted and diagonal striped bars represents the total reduced product concentration. Total summation of products is shown to increase with reaction time across all dosages according to Figure 12. Ammonia production, represented by the blue dotted bars, is shown in Figure 12 to increase with time for each dosage. Nitrite formation, represented by the green diagonal striped bars, is shown to decrease with increasing dosage in Figure 12. Figure 12A shows that at catalyst dosages of 12.5 mg/L and 25 mg/L, the concentration of nitrite does not decrease with time. At lower dosages an insufficient number of electrons were being provided by the catalyst for reduction.

3.3.3 Impact of Catalyst Dosage on Electron Capacity

A third parameter impacted by catalyst dosage was electron capacity. This was defined as the total number of electrons released from the catalyst and utilized to reduce nitrate to form nitrite, nitrogen gas, and ammonia. Electron capacity is measured in meq electrons/L.

$$NO_3^- + 2H^+ + 2e^- \rightarrow NO_2^- + H_2O \quad (18)\ ^{44}$$

$$NO_3^- + 10H^+ + 8e^- \rightarrow NH_4^+ + 3H_2O \quad (19)\ ^{44}$$

$$2NO_3^- + 12H^+ + 10e^- \rightarrow N_2 + 6H_2O \quad (20)\ ^{44}$$

$$electron\ capacity = (\Delta NO_2^-) \times \left(\frac{2}{14}\right) + (\Delta N_2) \times \left(\frac{5}{14}\right) + (\Delta NH_4^+) \times \left(\frac{8}{14}\right) \quad (21)\ ^{44}$$

$$\Delta NO_2^- = [NO_2^-]_t - [NO_2^-]_0 \quad (22)\ ^{44}$$

$$\Delta N_2 = [N_2]_t - [N_2]_0 \quad (23)\ ^{44}$$

$$\Delta NH_4^+ = [NH_4^+]_t - [NH_4^+]_0 \quad (24)\ ^{44}$$

Using the data from Figure 12, the number of electrons used for reduction was calculated for each catalyst dosage. The number of electrons used for reduction was defined as the electron capacity for each dosage. Electron capacity was plotted versus catalyst dosage in Figure 13.

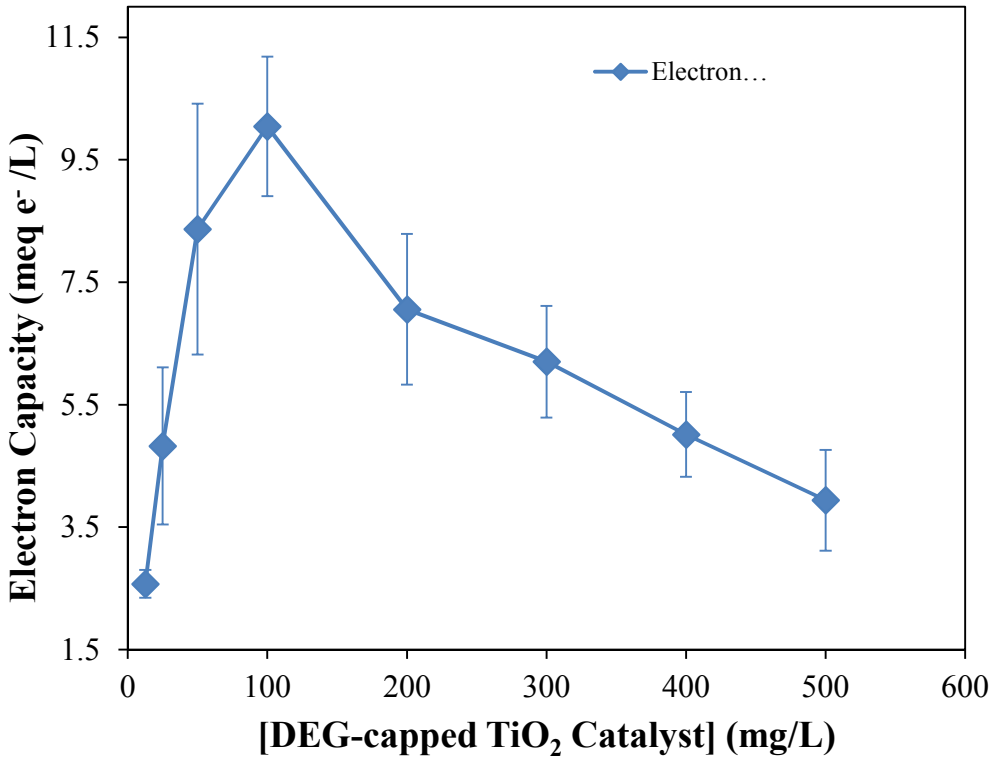

Figure 13. Impact of DEG-capped TiO_2 catalyst dosage on electron capacity. Initial NO_3^- concentration was 23 mg-N/L. A 6 mM phosphate buffer was used that maintained a pH 7.2. Ionic strength was 15 mM. DEG-capped TiO_2 of concentration 50 mg/L was used.

Figure 13 shows that the electron capacity reached maximum value at a catalyst dosage of 100 mg/L. Decreasing the catalyst dosage below 100 mg/L led to a reduction in electron capacity, while increasing the catalyst dosage beyond 100 mg/L also led to a reduction in electron capacity. The diminished electron capacity at dosages below 100

ppm was expected due to insufficient electron generation at lower concentrations of catalyst. The diminished electron capacity at higher dosages was unexpected. Higher dosages of catalyst were expected to generate a larger quantity of electrons and a higher electron capacity. It is speculated that at higher dosages the electrons from the catalyst were being consumed by other processes and not being used for reducing nitrate. Although at higher dosages there were more electrons generated, more were diverted to other processes and not included in the electron capacity calculation.

The rate constants for different dosages were also calculated. The ln [Nitrate] vs. time was plotted for all catalyst dosages in Figure 14. A linear regression was calculated to get a linear equation relating ln $[nitrate]_t$ vs. time. The slope for each linear regression was obtained and multiplied by -1 to get $k_{apparent}$. The $k_{intrinsic}$ rate constant was defined as $k_{apparent}$ divided by catalyst dosage.

$$\frac{d[NO_3^-]}{dt} = -k_{intrinsic} \times [NO_3^-] \times [catalyst] \quad (25)$$

$$[NO_3^-] = concentration\ of\ NO_3^-\ at\ time\ t \quad (26)$$

$$k_{intrinsic} \times [catalyst] = k_{apparent} \quad (27)$$

$$\frac{d[NO_3^-]}{dt} = -k_{apparent} \times [NO_3^-] \quad (28)$$

$$\ln\left(\frac{[NO_3^-]_t}{[NO_3^-]_0}\right) = -k_{apparent} \times t \quad (29)$$

$$-1 \times slope = k_{apparent} \quad (30)$$

$$k_{apparent} = \frac{k_{intrinsic}}{[Catalyst]} \quad (31)$$

The $k_{apparent}$ and $k_{intrinsic}$ values are listed in Table 3.

Table 3. Impact of catalyst dosage on $k_{apparent}$ and $k_{intrinsic}$. Initial NO_3^- concentration was 23 mg-N/L. A 6 mM phosphate buffer was used that maintained a pH 7.2. Ionic strength was 15 mM.

[Catalyst] (mg/L)	$k_{apparent} \times 10^{-3}$ **(s^{-1})**	$k_{intrinsic} \times 10^{-6}$ **$L \times mg^{-1} \times s^{-1}$**
12.5	3.7	296
25	5.6	224
50	8.1	162
100	6.2	62
200	3.9	20
300	2.9	9.7
400	2.4	6
500	1.7	3.4

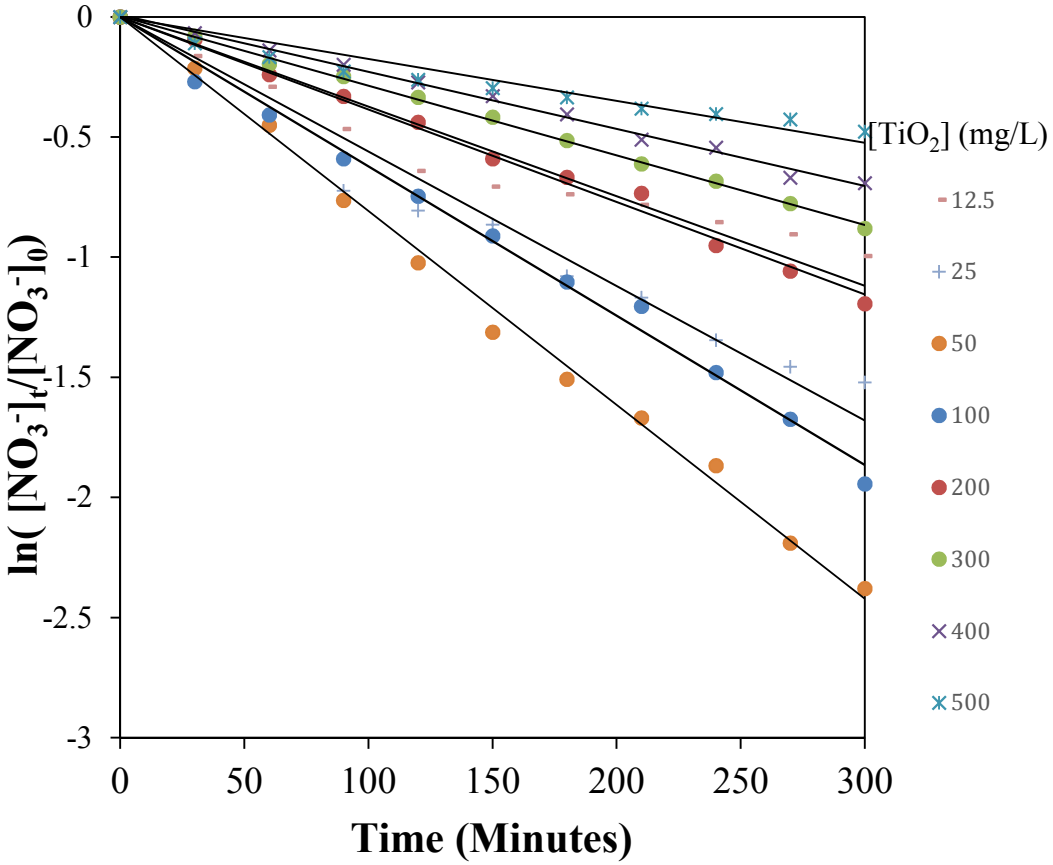

Figure 14. Impact of catalyst dosage on $k_{apparent}$. A linear regression is performed for each of the catalyst dosages. A 6 mM phosphate buffer was used that maintained a pH 7.2. Ionic strength was 15 mM. DEG-capped TiO_2 concentration of 50 mg/L was used.

Figure 14 shows that $k_{apparent}$ was the greatest at a dosage of 50 mg/L catalyst. The values in Table 3 show that $k_{apparent}$ decreased as the dosage increased above 50 mg/L or decreased below 50 mg/L. The value of $k_{intrinsic}$ for each catalyst dosage was derived from $k_{apparent}$ by dividing $k_{apparent}$ by the catalyst dosage. As catalyst dosage increased, the denominator in the expression for $k_{intrinsic}$ increased in value also. From 50 mg/L to 500 mg/L, $k_{apparent}$ decreased with increasing dosage. As a result, the calculated $k_{intrinsic}$ value decreased also. From 12.5 mg/L to 50 mg/L, $k_{apparent}$ increased in value. The rate at which $k_{apparent}$ increased was less than the rate at which catalyst dosage

increased. The ratio of $k_{apparent}$: catalyst dosage decreased also when catalyst dosage increased from 12.5 mg/L to 50 mg/L. Therefore, $k_{intrinsic}$ decreased continually as the dosage of catalyst increased from 12.5 mg/L to 500 mg/L.

3.4 Impact of Solution Matrix

The next parameter investigated was the solution matrix. This parameter was investigated to determine the feasibility of catalyst usage in actual ground water chemical conditions. Table 4 lists the constituents of synthetic groundwater. The performance of the catalyst was compared in ground water chemical conditions and compared to results in DI water.

Table 4. Table of constituents of synthetic water matrix. DEG-capped TiO_2 concentration 50 mg/L was used. [45]

Parameter	Mean (mg/L)	Parameter	Mean (mg/L)
EC (uS/cm)	235.1	**Mg^{2+}**	6.0
pH	6.2	**Cl^-**	13.1
NO_3^-	40.3	**HCO_3^-**	37.9
Na^+	13.6	**SO_4^{2-}**	32.9
K^+	3.9	**SiO_2**	36.6
Ca^{2+}	24.4	**Dissolved organic carbon**	1.6

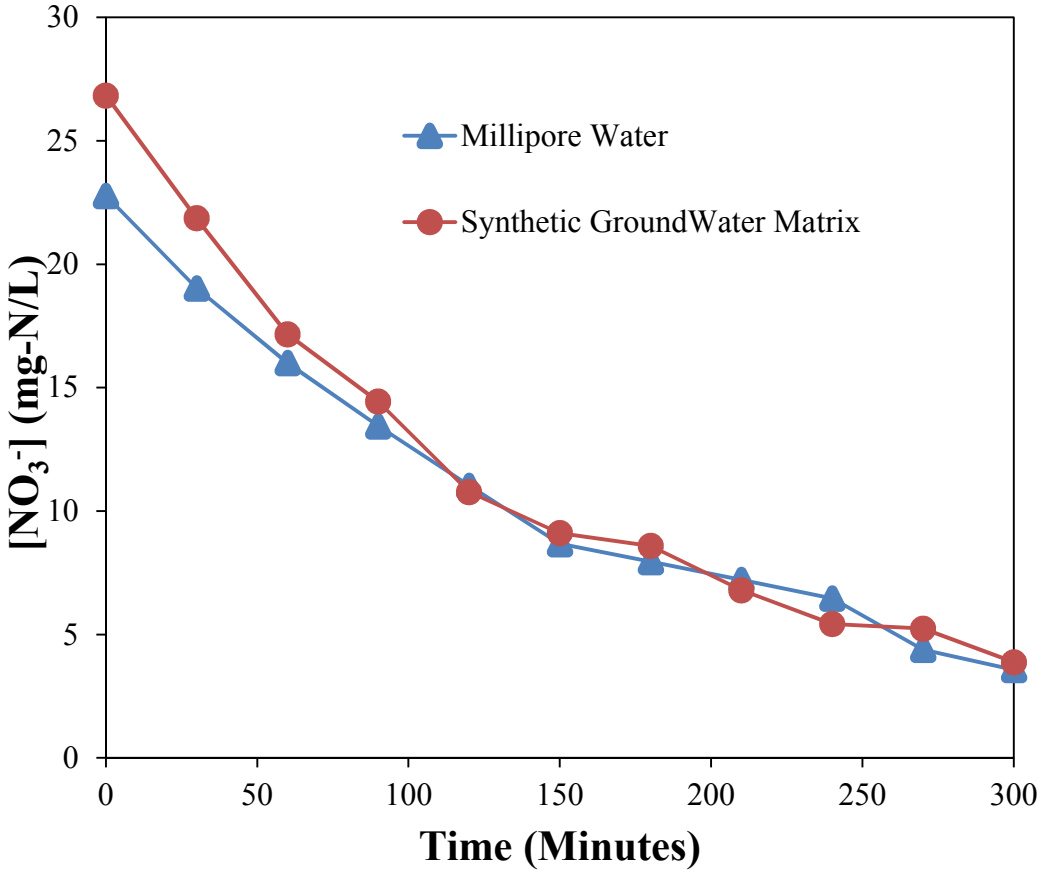

Figure 15. Impact of water matrix upon catalyst performance towards reduction of nitrate. The amount of nitrate remaining is plotted as a function of time in Millipore water and a synthetic water matrix. Initial [NO_3^-] was 23 mg-N/L. A 6 mM phosphate buffer was used that maintained a pH 7.2. Ionic strength was 15 mM. DEG-capped TiO_2 concentration 50 mg/L was used. [45]

Figure 15 shows that the catalyst was effective in removing nitrate in synthetic groundwater conditions. DEG-capped TiO_2 was not limited to waters with pristine conditions but is also applicable to water with conditions that simulate groundwater.

3.5 Impact of Initial Nitrate Concentration

The effect of contaminant concentration upon catalyst performance was the next parameter evaluated. This parameter was chosen for analysis because knowing how nitrate concentration affects catalyst performance is important in determining the concentration levels over which the catalyst is effective. The performance of the catalyst was based on nitrate levels reduced and electron capacity. The prediction is that as initial nitrate concentration increases, delta nitrate will increase along with electrons.

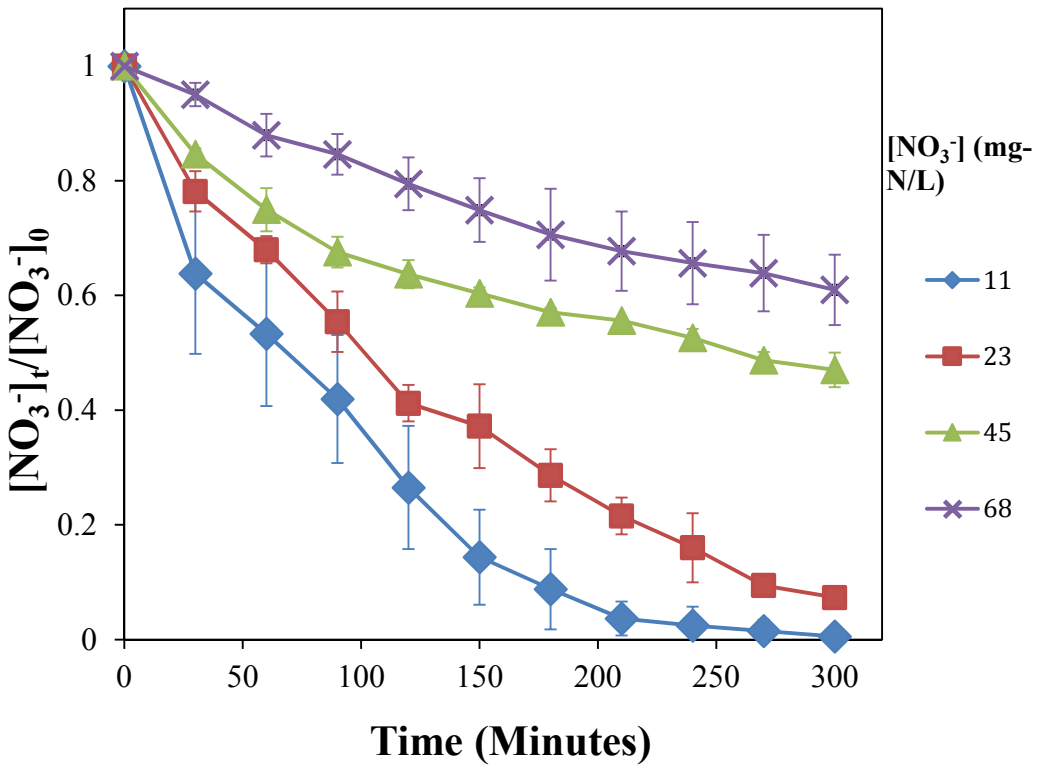

Figure 16. Impact of initial nitrate concentration on nitrate reduction. C/C_0 for nitrate was plotted as a function of time for initial nitrate concentrations of 11 mg-N/L, 23 mg-N/L, 45 mg-N/L, and 68 mg-N/L. A 6 mM phosphate buffer was used that maintained a pH 7.2. Ionic strength was 15 mM. DEG-capped TiO_2 concentration of 50 mg/L was used.

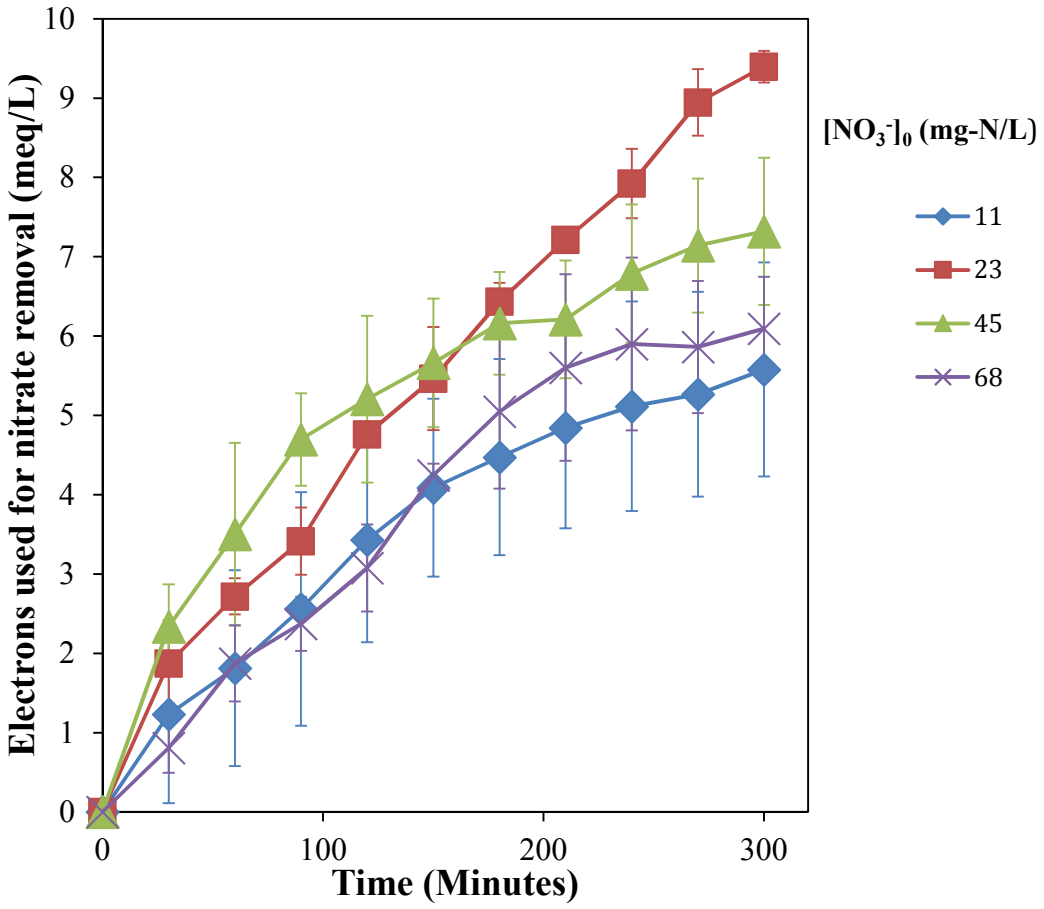

Figure 17. Impact of initial nitrate concentration on electrons used for reduction. Electrons uses were plotted as a function of time for initial nitrate concentrations of 11 mg-N/L, 23 mg-N/L, 45 mg-N/L, and 68 mg-N/L. A 6 mM phosphate buffer was used that maintained a pH 7.2. Ionic strength was 15 mM. DEG-capped TiO_2 concentration of 50 mg/L was used.

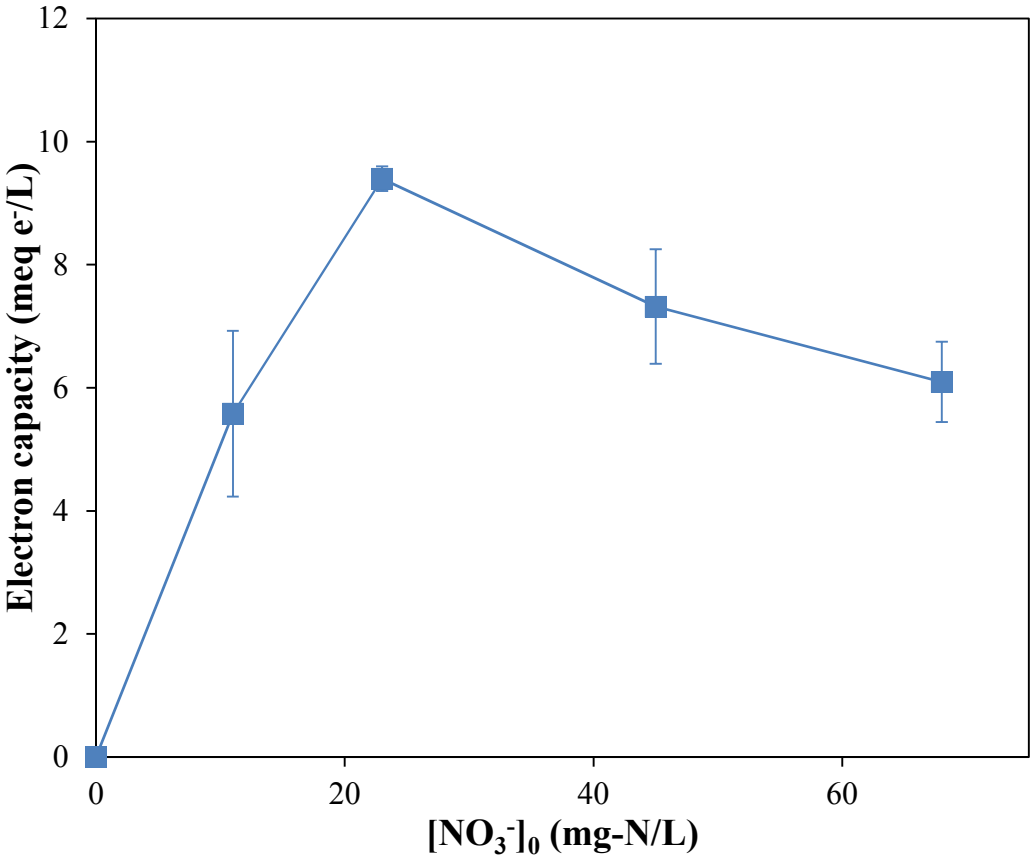

Figure 18. Impact of different initial nitrate concentrations on electron capacity of catalyst over 300 minutes. Electron capacity was plotted as a function of initial nitrate concentration at values of 11 mg-N/L, 23 mg-N/L, 45 mg-N/L, and 68 mg-N/L. A 6 mM phosphate buffer was used that maintained a pH 7.2. Ionic strength was 15 mM. DEG-capped TiO_2 concentration of 50 mg/L was used. Duration of experiment was 300 minutes.

Electron capacity was defined to be the quantity of electrons that were used for reduction of nitrate and its products. Electron capacity was calculated for Figures 18-19 using the same equation as in Figure 13.

$$electron\ capacity = (\Delta NO_2^-) * \left(\frac{2}{14}\right) + (\Delta N_2) * \left(\frac{5}{14}\right) + (\Delta NH_4^+) * \left(\frac{8}{14}\right) \quad (28)\ [44]$$

The results from Figures 17 and 19 show that as the concentration of initial nitrate increases, the quantity of nitrate reduced decreases along with electron capacity. A possible explanation was that at higher initial nitrate concentrations led to a greater scavenging of electrons by other process. Hydroxyl radical formation was thought to be the process scavenging photo generated electrons. Steady-state concentrations of hydroxyl radical ($[\cdot OH]_{ss}$) were calculated using phenol as a probe.[42] Phenol decay was assumed to be a pseudo-first order reaction with respect to phenol.[42] Figure 19 plots the semi-ln of phenol concentration vs. time.

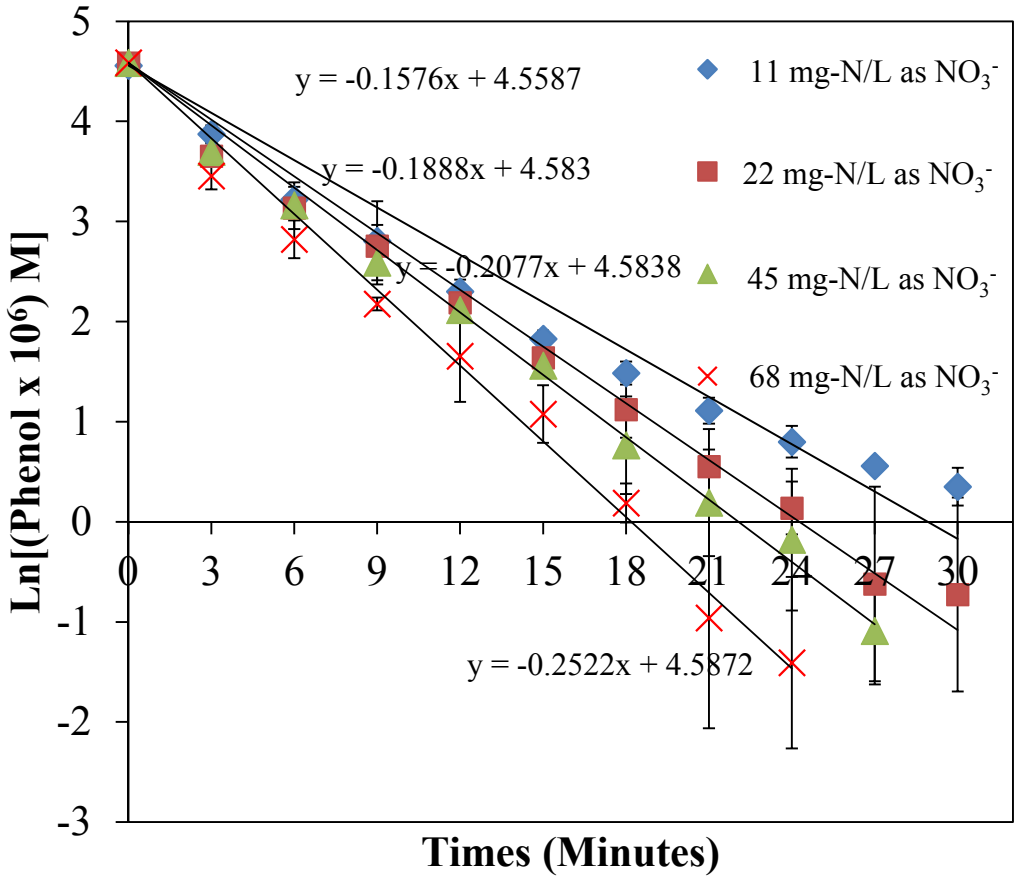

Figure 19 Impact of nitrate concentration on phenol decay over 30 minutes. A 6 mM Phosphate buffer was used that maintained pH at 7.2 with ionic strength at 15 mM.

Figure 19 provides the pseudo first order rate constant, k_{obs}, for each initial nitrate concentration. Using Equations 9-12, $[\cdot OH]_{ss}$ values are calculated. Figure 20 plots $[\cdot OH]_{ss}$ versus initial nitrate concentration after 30 minutes.

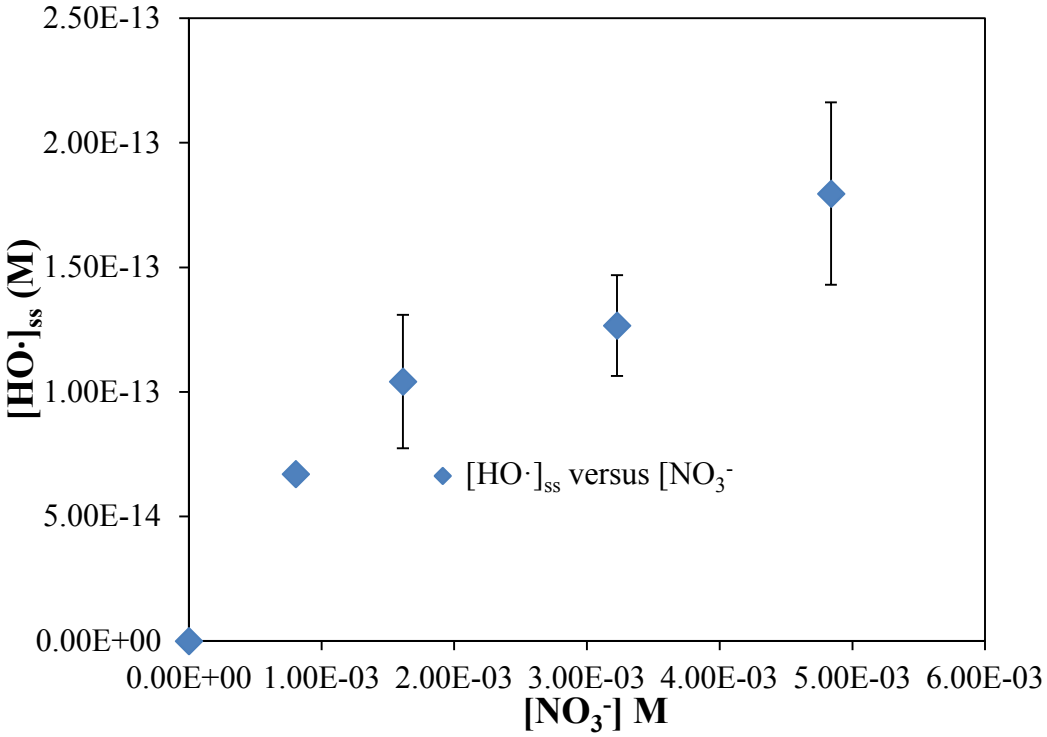

Figure 20 Impact of nitrate concentration in hydroxyl radical steady state concentration over 30 minutes. A 6 mM phosphate buffer was used that maintained a pH 7.2. Ionic strength was 15 mM. Duration of the experiment was 30 minutes.

When hydroxyl radical concentration reaches its steady state, the rate of change of hydroxyl radicals is zero. The rate at which hydroxyl radical concentration changes is given by equation 32.

$$\frac{d[\cdot OH]}{dt} = k_1 \times [NO_3^-] - k_2 \times [Phenol] \times [\cdot OH] \qquad (32)^{42}$$

The product $k_1 \times [NO_3^-]$ equals the rate at which hydroxyl radicals are generated from nitrate, and the product $k_2 \times [Phenol] \times [\cdot OH]$ is equal to the rate at which hydroxyl radicals are consumed by reaction with phenol. When $d[\cdot OH]/dt$ is zero, $[\cdot OH] = [\cdot OH]_{ss}$ and the rate of hydroxyl production and consumption are equal. Setting $d[\cdot OH]/dt$ to zero and rearranging equation 32, the rate at which hydroxyl radicals are generated from nitrate can be calculated from equation 33 through measurement of hydroxyl radical consumption.

$$k_1 \times [NO_3^-] = k_2 \times [Phenol] \times [\cdot OH]_{ss} \qquad (33)^{42}$$

The graph of $k_2 \times [Phenol^-] \times [\cdot OH]_{ss}$ (uM/s) vs. $[NO_3^-]$ (mM) is plotted in figure 20. A linear regression is performed in figure 20 to calculate the slope. The slope calculated is equal to $k_1 \times 1000$.

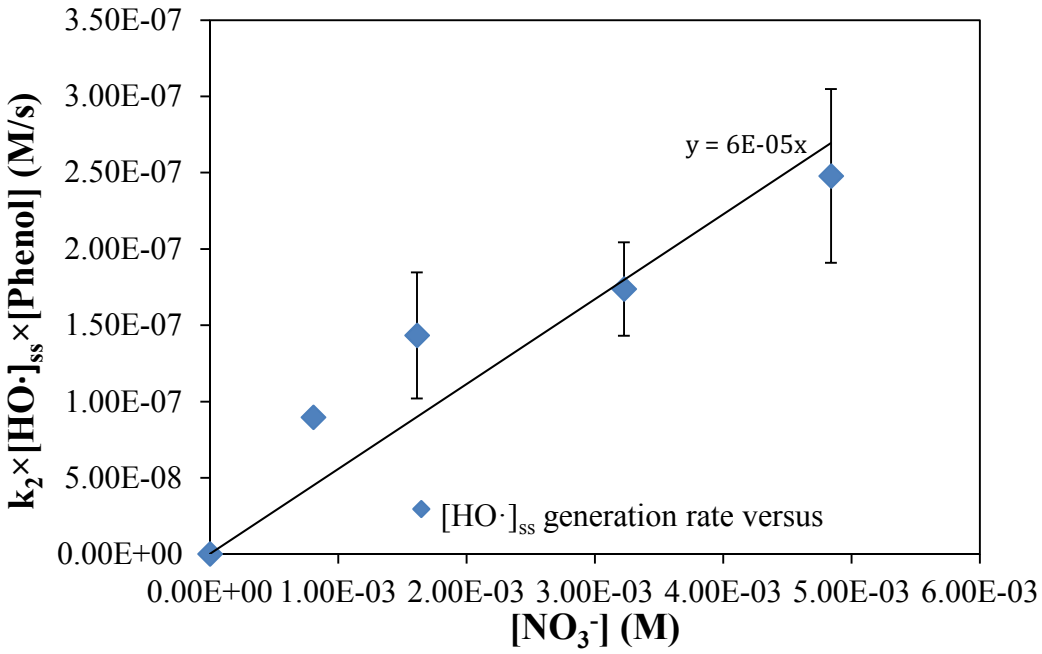

Figure 21. Impact of nitrate concentration on hydroxyl radical generation over 30 minutes. A 6 mM phosphate buffer was used that maintained a pH 7.2. Ionic strength was 15 mM. Duration of the experiment was 30 minutes.

The slope calculated in Figure 21 was equal to 0.00006. This k_1 value was combined with the previous data from Figure 16 to calculate the hydroxyl radical concentration generated over the duration of the experiment. The 5-hour experiment was divided into 10 intervals that spanned 30 minutes each. During each 30-minute time interval, normalized $[NO_3^-]$ was calculated by averaging the $[NO_3^-]$ at the beginning and end of the 30 minute interval. Equation 34 shows this calculation for average $[NO_3^-]$ from time t_1 to time t_2 as:

$$Average\ [NO_3^-]_{t1-t2} = 0.5 \times ([NO_3^-]_{t1} + [NO_3^-]_{t2}) \qquad (34)$$

The amount of hydroxyl radicals generated from time t_1 to time t_2 is given by Equation 35.

$$[HO\cdot]_{ss}(t_2 - t_1) = k_1 \times 60 \times (t_2 - t_1) \times Average\ [NO_3^-]_{t1-t2} \qquad (35)$$

The amount of hydroxyl radicals generated over 5 hours is calculated by summing the hydroxyl radicals from the 10 30 minute time intervals as seen in Equation 36.

$$\int_0^{300}[HO\cdot]_t dt = ([HO\cdot]_{0-30} + [HO\cdot]_{30-60} + [HO\cdot]_{60-90} + [HO\cdot]_{90-120} + [HO\cdot]_{120-150} + [HO\cdot]_{150-180} + [HO\cdot]_{180-210} + [HO\cdot]_{210-240} + [HO\cdot]_{240-270} + [HO\cdot]_{270-300}) \times 1800 \qquad (36)$$

The $[HO\cdot]_t$ is calculated for the four initial $[NO_3^-]$ and is listed in Table 5.

Table 5 [HO·] generation versus initial [Nitrate] (mg-N/L)

Initial [Nitrate] (mg-N/L)	[HO·] $\times 10^3$ M
0	0
11	0.055
22	0.17
45	0.53
68	1.05

Table 5 shows that concentration of [HO·] generated after 5 hours when initial [NO_3^-] is 68 mg-N/L was .70 mM. The concentration of [HO·] generated after 5 hours when initial [NO_3^-] is 11 mg-N/L was 0.037 mM. It is assumed that the stoichiometric ratio of hydroxyl radical and electron reaction is one to one, therefore each hydroxyl radical can scavenge one electron. Figure 22 combines the data from Table 5 and Figure 18 to include the scavenging effect of hydroxyl radicals.

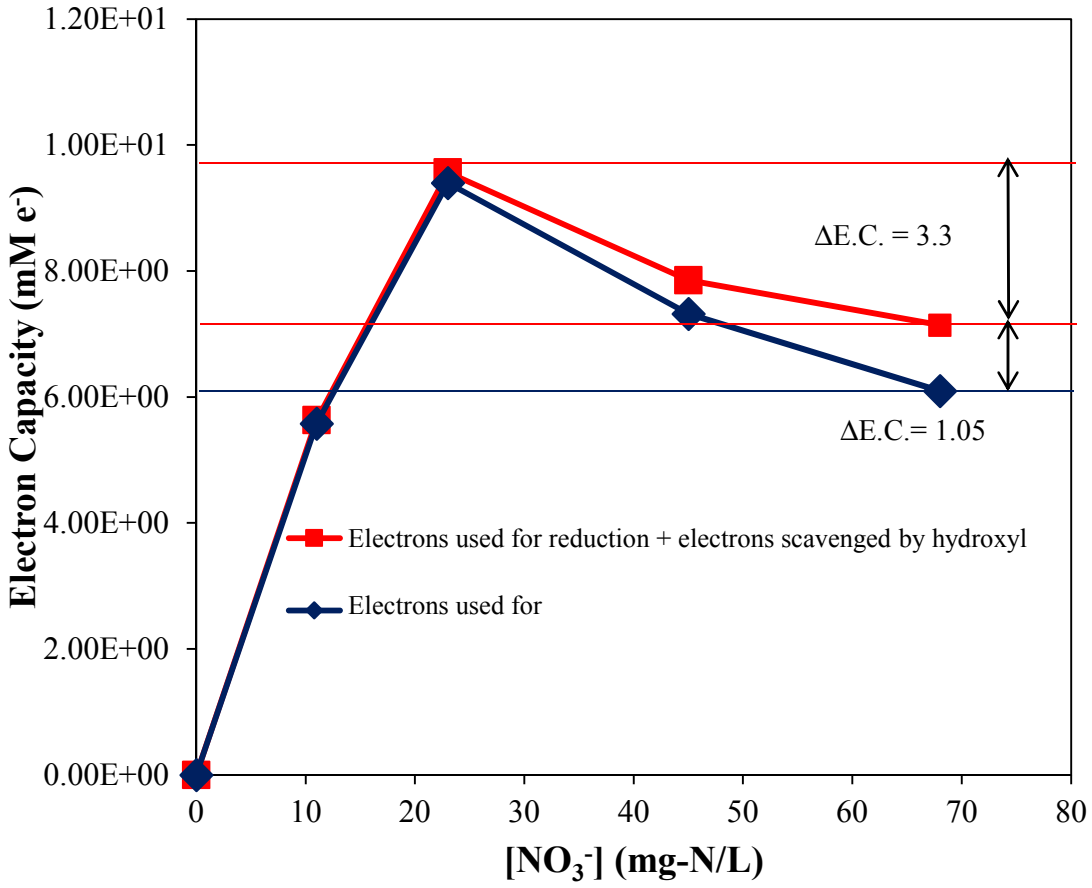

Figure 22. Impact of hydroxyl radical scavenging on calculation of electron capacity. A 6 mM phosphate buffer was used that maintained a pH 7.2. Ionic strength was 15 mM. DEG-capped TiO_2 concentration of 50 mg/L was used.

The red curve in Figure 22 represents electron capacity calculated including electrons lost due to hydroxyl radical scavenging. The blue curve is from Figure 18 and does not include the effect of hydroxyl radical scavenging. The difference in electron capacity from Figure 18 at initial nitrate concentrations 68 mg-N/L and 23 mg-N/L was 3.3 mM. The difference in hydroxyl radical generation at initial nitrate levels of 23 mg-N/L and 68 mg-N/L was 0.88 mM. Hydroxyl radical scavenging can only account for 31.6% of the difference in electron capacities at initial nitrate concentrations of 23 mg-N/L and 68 mg-

N/L. Therefore, hydroxyl radical scavenging of electrons cannot account for the diminished electron capacity at higher initial nitrate concentrations. The relationship between electron capacity and nitrate concentration requires further investigation.

3.6 Application of TiO_2 to Bromate Removal

In addition to seeing the effectiveness of DEG-capped TiO_2 on nitrate reduction, its effectiveness toward bromate reduction was also evaluated. Bromate is another oxyanion contaminant with a similar redox potential as nitrate.[44] Figure 22 shows bromate reduction vs. time using DEG-capped TiO_2. The reduction of bromate to bromide is give in equation 32.

$$BrO_3^- + 6H^+ + 6e^- \rightarrow Br^- + 3H_2O \qquad E°_H = 1440 \text{ mV} \quad (37)[44]$$

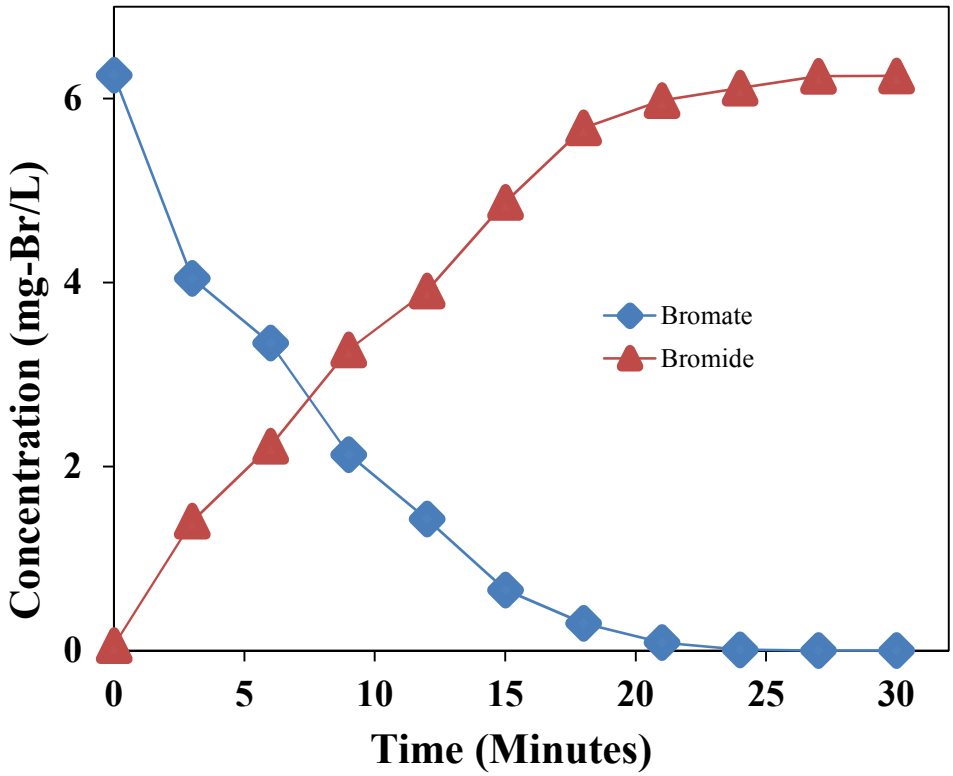

Figure 23. DEG-capped TiO_2 reduction of bromate with bromide formation. Bromate and bromide concentration were plotted as a function of time. A 6 mM phosphate buffer was used that maintained a pH 7.2. Ionic strength was 15 mM. DEG-capped TiO_2 concentration of 50 mg/L was used. Initial BrO_3^- concentration was 6.3 mg-Br/L.

Figure 23 shows that the catalyst was also effective in reducing bromate. After 30 minutes, 100% of the Bromate was reduced. The product distribution of bromate after 30 minutes was 99% bromide.

3.7 Application of TiO_2 to Perchlorate Removal

The effectiveness of DEG-capped TiO_2 for reducing perchlorate was also evaluated. At 50 mg/L catalyst concentration perchlorate was not being reduced appreciably. The catalyst dosage was increased to 500 and 1000 mg/L. The results are shown in Figure 24.

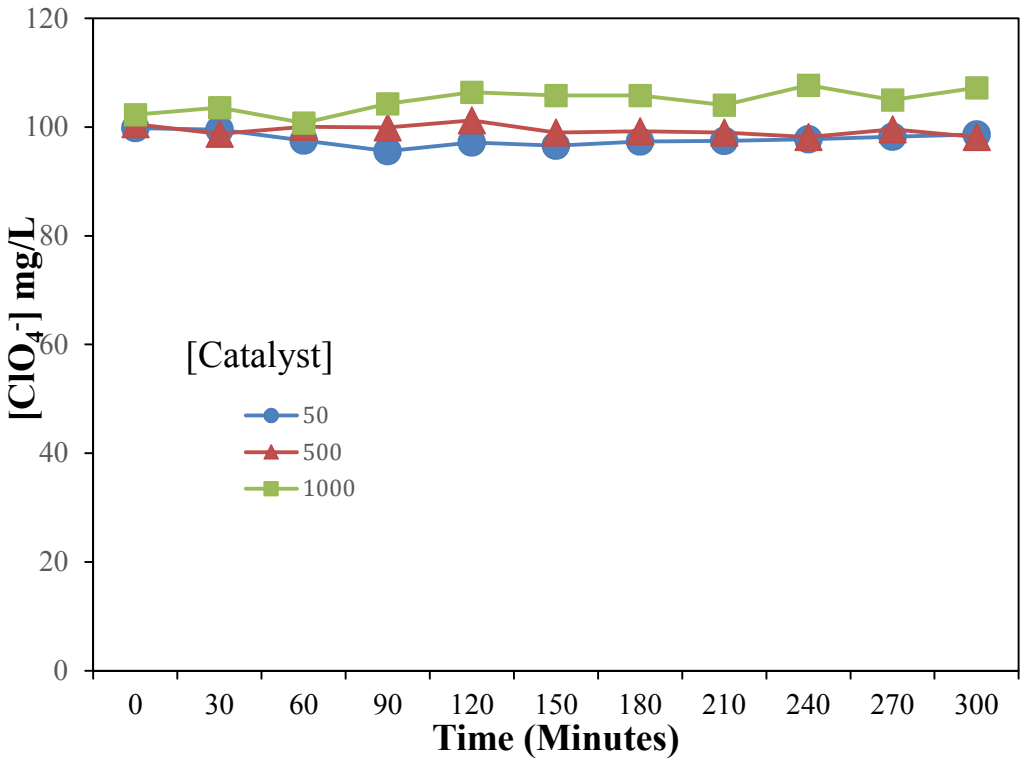

Figure 24. DEG-capped TiO_2 reduction of ClO_4^-. A 6 mM phosphate buffer was used that maintained a pH 7.2. Ionic strength was 15 mM. DEG-capped TiO_2 concentration of 50 mg/L was used. Initial ClO_4^- concentration was 100 mg-ClO_4^-/L

Figure 24 shows that DEG-capped TiO_2 was not effective at reducing perchlorate. Increasing the dosage from 50 to 500 to 1000 mg/L seemed to have no effect. The

reduction potentials of nitrate (NO_3^-), bromate (BrO_3^-) and perchlorate (ClO_4^-) are given in Equations 37, 38, 39, and 40.

$$2NO_3^- + 12H^+ + 10e^- \rightarrow N_2 + 6H_2O \qquad E°_H = 1225 \text{ mV} \quad (38)[44]$$

$$ClO_4^- + 8H^+ + 8e^- \rightarrow Cl^- + 4H_2O \qquad E°_H = 1280 \text{ mV} \quad (39)[46]$$

$$ClO_4^- + 2H^+ + 2e^- \rightarrow ClO_3^- + H_2O \qquad E°_H = 250 \text{ mV} \quad (40)[46]$$

Nitrate, bromate and perchlorate have redox potentials that are similar in value. The reduction of perchlorate therefore should be thermodynamically favorable as are the reductions of bromate and nitrate. The synthesized TiO_2 catalyst was able to reduce bromate and nitrate, but there was no reduction of perchlorate. This is likely due to the slow kinetics of reduction of perchlorate by TiO_2. The reductions of nitrate and bromate in contrast were thermodynamically and kinetically favorable. Therefore there was observable reduction of nitrate and bromate by the synthesized TiO_2 but no observed reduction of perchlorate.

Chapter 4: Conclusion

The overall goal of this research was to investigate the effectiveness of synthesized titanium dioxide (TiO_2) on the reductive removal of nitrate and other chemical contaminants. The effectiveness of synthesized TiO_2 was examined through 1) the comparison of TiO_2 nanoparticles synthesized under different conditions; 2) the comparison of nitrate reduction by synthesized TiO_2 under different experimental conditions; and 3) the ability of synthesized TiO_2 to reduce other contaminants.

In Chapter 3.1, the performance of 3 different TiO_2 catalysts: P25 TiO_2, Ba-doped TiO_2 and DEG-capped TiO_2, were evaluated based on reduction of nitrate over time. Nitrate concentrations were quantified using ion chromatography (IC). The results of nitrate reduction showed that both barium-doped TiO_2 and DEG-capped TiO_2 were noticeably more effective at reducing nitrate when compared to P25 TiO_2. A t-test was performed to compare the results obtained from the barium-doped TiO_2 and the DEG-capped TiO_2. The results showed that at all measured points, the mean value of nitrate concentration for Ba-doped TiO_2 did not differ significantly at the 95% confidence limit from the mean value of nitrate concentration for DEG-capped TiO_2. It can be concluded that the addition of Ba-doped did not lead to a significant increase in nitrate reduction. These findings suggest that DEG solvent used for DEG-capped TiO_2 was able to provide sufficient electrons for hole scavenging. For subsequent studies, only the DEG-capped TiO_2 was used.

Chapter 3.2 investigated the role of synthesis parameters on nitrate reduction. Nitrate reduction was performed by DEG-capped catalysts synthesized under 4 different conditions. The 4 conditions were distinguished by $TiCl_4$ concentration and hydrolysis heating time. First order rate constants for nitrate removal were calculated for the 4 conditions. Results suggested that there was an optimum set of conditions for catalyst synthesis. The optimum $TiCl_4$ concentration was found to be 89 mM. Decreasing the $TiCl_4$ concentration through addition of excess water lowered the calculated first order rate constant. These findings suggest that water may have a negative effect on catalyst performance possibly through blockage of DEG-capping to the TiO_2 crystal structure. The optimum heating time during hydrolysis was determined to be 3 hours. Decreasing of the heating time during hydrolysis to 2 hours decreased the first order rate constant. Increasing the heating time during hydrolysis to 6 hours also led to a decreased first order rate constant.

Chapter 3.3 investigated the role of catalyst dosage on nitrate reduction, product distribution and electron capacity. Results suggested a non-linear relationship between catalyst dosage and nitrate reduction. Data indicated there was an optimum dosage of 50 mg/L catalyst for nitrate reduction. Deviations from this value resulted in decreased nitrate reduction. Results from product distribution measurements showed that as catalyst dosage increased, nitrite formation decreased. This trend was thought to be at attributed to insufficient electrons being provided by the catalyst at lower dosages. Results from electron capacity measurements show a non-linear relationship between electron capacity and catalyst dosage. Data indicated there was an optimum dosage of 100 mg/L catalyst.

This finding indicates that at higher dosages electrons are being used for another process besides reduction of nitrate.

Chapter 3.4 investigated the impact of solution matrix. The results suggest that the performance of the catalyst remains the same whether it is employed in pristine water conditions or if it is used in water conditions that simulate actual groundwater.

Chapter 3.5 investigated the impact of initial NO_3^- concentration on nitrate reduction. The results suggested that the relationships between initial nitrate concentration and nitrate reduction and initial nitrate concentration and electron capacity were non-linear. These results were opposite to what was originally predicted. It was predicted that increasing initial nitrate concentration would lead to increases in nitrate reduction and electron capacity. It was proposed that increased hydroxyl radical formation at greater initial nitrate concentrations was responsible for the decrease in electron capacity seen at larger initial nitrate concentration. The results from the phenol degradation experiments showed that the increase in hydroxyl radical steady concentrations at higher initial nitrate concentrations was not sufficient to explain the difference in electron capacity.

Chapters 3.6 and 3.7 investigated how effective the synthesized TiO_2 was able to reduce the contaminants bromate (BrO_3^-) and perchlorate (ClO_4^-). The results from chapter 3.6 indicated that the catalyst was effective at reducing bromate with 100% of bromate reduced and 99% of the products in the form of bromide. The results from chapter 3.7 indicate that the catalyst is ineffective in reducing perchlorate. Increasing the dosage of catalyst from 50 mg/L to 1000 mg/L had no positive effect on the reduction of

perchlorate. The results of chapters 3.6 and 3.7 indicate that the catalyst has versatility in its ability to reduce certain contaminants but that other contaminants prove to be recalcitrant towards reduction from the catalyst.

References

1) Kenny, J.F.; Barber, N.L.; Hutson, S.S.; Linsey, K.S.; Lovelace, J.K.; Maupin, M.A., 2009, Estimated use of water in the United States in 2005: U.S. Geological Survey Circular 1344, 52 p.

2) Esser, B.; Hudson, B.; Moran, J., Beller, H., Carlsen, T., Dooher, B., Krauter, P., Mcnab, W., Madrid, V., Rice, D., Verce, M. Nitrate contamination in California groundwater: an integrated approach to basin assessment and resource protection. U.S. Department of Energy Lawrence Livermore National Laboratory, 2002.

3) Puckett, L.J. *Nonpoint and Point Sources of Nitrogen in Major Watersheds of the United States*; U.S. Geological Survey Water Resources Investigations Report 94-4001, 1994.

4) Cortez, S.; Teixeira, P.; Oliveira, R.; Mota, M. Denitrification of a landfill leachate with high nitrate concentration in an anoxic rotating biological contactor. *Biodegradation*. **2011**, *22* (3), 661-671.

5) National Research Council. *Drinking Water and Heatlh, Volume 1.* Washington, DC: The National Academies Press, 1977. Doi:10.17226/1780

6) Lee, C.C. *Environmental Engineering 4th Edition*. Lanham: The Scarecrow Press, Inc., 2005. Print

7) Rosenstock T.; Liptzin D.; Six J, Tomich T. Nitrogen fertilizer use in California: Assessing the data, trends and a way forward. *California Agriculture*. **2013**, *67* (1):68-79. DOI: 10.3733/ca.E.v067n01p68.

8) Nehring, Richard. "Fertilizer Use and Markets."*United State Department of Agriculture Economic Research Service*. 12 July 2013. Friday 29 August, 2015. < http://www.ers.usda.gov/topics/farm-practices-management/chemical-inputs/fertilizer-use-markets.aspx>

9) Fewtrell, L. Drinking Water Nitrate, Methemoglobinemia, and Global Burden of Disease: A Discussion. *Environmental Health Perspectives*. **2004**, *112* (14), 1371-1374.

10) Brunning-Fann, C.S.; Kaneene J.B. The effects of nitrate, nitrite, and N-nitroso compouns on human health: a review *Vet Hum Toxicol*. **1994.** 35(6): 521-538.

11) Fan, A.M.; Willhite, C.C; Book S.A .Evaluation of the nitrate drinking water standard with reference to infant methemoglobinemia and potential reproductive toxicology. *Regul Toxicology Pharmacol*, **1987**. 7 (2): 135-148.

12) J.O. Lundberg, E. Weitzberg, NO-synthase independent NO generation in mammals, *Biochem. Biophys. Res. Commun*. **2010**. *396* (2010) 39–45.

13) Kapoor, A. and Viraghavan, T. Nitrate removal from drinking water - review. Journal of Environmental Engineering. **1997**, *123* (4), 371-380.

14) Korngold, E. Removal of nitrates from potable water by ion exchange. *Water Air Soil Pollution,* **1973**, *2* (1), 15-22.

15) Guter, G. Removal of nitrate from contaminated water supplies for public use. *EPA-600/S2-82-042*. **1982**. U.S. Envir. Protection Agency (EPA). Cincinnati, Ohio.

16) Green, M. and G. Shelef. *Treatment of nitrate contaminated groundwater for drinking purposes*, pp. 587-606. *In* U. Zoller (ed.) Groundwater contamination and control, Marcel Dekker Publishers, New York, 1994.

17) Shrimali, M., and K.P. Singh, New methods of nitrate removal from water. *Environmental Pollution*, **2001**. *112* (3), 351-359.

18) Reddy, K.J. and Lin, J. Nitrate removal from groundwater using catalytic reduction. *Water Research*, **2000**. *34* (3), 995-1001.

19) Kapoor, A. and Viraraghavan, T. Nitrate removal from drinking water - review. *Journal of Environmental Engineering*, **1997**, 123(4), 371-380.

20) Gonder, Z.B.; Kaya, Y.; Vergili, I.; Barlas, H. Capacity loss in an organically fouled ion exchanger. *Desalination*, **1999**. *189* (2-3), 303-307.

21) Solley, D.; Gronow, C.; Tait, S.; Bates, J.; Buchanan, A. Managing the reverse osmosis concentrate from the Western Corridor Recycled Water Scheme. *Water Practice and Technology,* **2010**. *5* (1), 1-8.

22) Perez-Gonzalez, A.; Urtiaga A.M.; Ibanez, R.; Ortiz, I. State of the art and review on the treatment technologies of water reverse osmosis concentrates. *Water Research*, **2012**. *46* (2), 267-283.

23) Knowles, R. Denitrification. *Microbiology Rev.*, **1982.** *46* (1), 4370.

24) Mateju, V.; Cizinska,, S.; Krejci, I.; Janoch, T. Biological denitrification- a review. *Enzyme Microbial Technolog*., **1992**. *14* (3), 170-183.

25) Clara, M.; Kreuzinger, N.; Strenn, B.; Gans, O.; Kroiss, H. The solids retention time—a suitable design parameter to evaluate the capacity of wastewater treatment plants to remove micropollutants. *Water Research*, **2005**. *39* (1), 97-106

26) Dey, A. Modeling Simultaneous Nitrification-Denitrification Process in an Activated Sludge Continuous Flow Stirred-Tank Reactor: System Optimization and Sensitivity Analysis. *Environmental Engineering Science*, **2010**. *27* (9), 757-764.

27) Hsu, J.C.; Liao, C.H.; Wei, L. Nitrate removal by synthetic nano-scale-zero-valent iron in aqueous recirculated reactor. *Sustain Environ. Res.* **2011**, *21* (6). 353-359.

28) Su, C.; Puls, R.W. Nitrate reduction by zerovalent iron: Effects of formate, oxalate, citrate, chloride, sulfate, borate, and phosphate. *Environmental Science and Technology*, **2004**, *38* (9). 2715-2720.

29) Liu, H.B.; Chen, T.H.; Chang, D.Y.; Chen, D.; Liu, Y.; He, H.P.; Yuan, P.; Frost, R. Nitrate reduction over nanoscale zero-valent iron prepared by hydrogen reduction of goethite. *Materials Chemistry and Physics*, **2012**. *133* (1), 205-211.

30) Park, H.; Park, Y.M.; Yoo, K.M.; Lee, S.H. Reduction of nitrate by resin-supported nanoscale zero-valent iron. *Water Science and Technology*, **2009**. *59* (11), 2153-2157.

31) Doudrick, K.; Yang, T.; Hristovski, K.; Westerhoff, P., "Photocatalytic nitrate reduction in water: Managing the hole scavenger and reaction by product selectivity." *Applied Catalyst B: Environmental.* **2013**. *136-137*. 40-47.

32) Lazar, M.A.; Varghese, S.; Nair, S.S. Photocatalytic Water Treatment by Titanium Dioxide: Recent Updates. *Catalysts*, **2012**, *2* (4), 572-601.

33) Zhai, H.J.; Wang, L.S. Probing the electronic structure and band gap evolution of titanium oxide clusters using photoelectron spectroscopy. *Journal of American Chemical Society*, **2007**, *129* (10), 3022-3026.

34) Yang, T.; Doudrick, K.; Westerhoff, P. Photocatalytic reduction of brine using titanium dioxide for regeneration of ion exchange brine. *Water Research*, **2013**, *47* (3), 1299-1307

35) Starr, R.C.; Gillham, R,W. Denitrification and organic carbon availability in two aquifers. *Groundwater*, **1993**, *31* (6), 934-947.

36) Wang, Lawrence K. and Nazih K. Shammas. *Water engineering: hydraulics, distribution, and treatment*. New Jersey: John Wiley & Sons, Inc., 2016. Print

37) Doudrick, K.; Monzon, O.; Mangonon, A.; Hristovski, K.; Westerhoff, P. Nitrate Reduction in Water Using Commercial Titanium Dioxide Photocatalysts (P25, P90, and Hombikat UV100). *Journal of Environmental Engineering*, **2012**, *138* (8), 852-861.

38) Wang, W.; Ye, Y.; Feng, J.; Chi, M.; Guo, J.; Yin, Y. Enhanced Photoreversible Color Switching of Redox Dyes Catalyzed by Barium-Doped TiO_2 Nanocrystals. *Angewandte Chemie*, **2015**, *127*, 1337-1342

39) Wang, W.; Ye, M.; He, L.; Yin, Y. Nanocrystalline TiO_2-Catalyzed Photoreversible Color Switching. *Nano Letters*. **2014**, *14* (3), 1681-1686.

40) Xu, Y., *Ferromagnetic Materials and their Applications*. Elsevier Science Publications, 1991. Print

41) Rice, E.W.; Rodger B. Baird; Andrew D. Eaton, and Lenore S. Clesceri. *Standard Methods For the Examination of Water and Wastewater-22nd Edition*. Washington, DC: American Public Health Association, 2012. Print

42) Kochany, J.; Bolton, J.R. Mechanism of photodegradation of aqueous organic pollutants. 1. EPR spin-trapping technique for the determination of hydroxyl radical rate constants in the photooxidation of chlorophenols following the photolysis of hydrogen peroxide. *The Journal of Physical Chemistry*, **1991**, *95* (13), 5116-5120

43) Lan, C.M.; Liu, S.E.; Shiou, J.W.; Hu, J.Y.; Lin, M.H.; Diau, E.W. Formation of size-tunable dandelion-like hierarchical rutile titania nanospheres for dye-sensitized solar cells. *RSC Advances*, **2013**, *3*, 559-565

44) Benjamin, M.M., *Water Chemistry*. Ottawa: Waveland Press, 2015. Print

45) Babiker I S, Mohamed M A A, Terao H, et al. Assessment of groundwater contamination by nitrate leaching from intensive vegetable cultivation using geographical information system. *Environment International*, **2004**, *29* (8): 1009-1017.

46) Bardiya, N.; Bae, J. Dissimilatory perchlorate reduction. A review. *Microbiological Research*, **2011**, *166* (4), 237-254.